EFFECTS OF MAINSHOCK-AFTERSHOCK SEQUENCES ON FRAGILITY ANALYSIS OF RC BUILDINGS WITH AGEING

Di Sarno, L.,
Senior Lecturer in Structural and Earthquake Engineering, Institute for Risk and Uncertainty, School of Engineering, University of Liverpool, Liverpool, UK. Email address: Luigi.Di-sarno@liverpool.ac.uk

Pugliese, F.,
PhD Candidate in Seismic Analysis and Risk Assessment, Institute for Risk and Uncertainty, School of Engineering, University of Liverpool, Liverpool, UK. Email address: Francesco.Pugliese@liverpool.ac.uk.

Abstract:

This paper presents the seismic vulnerability assessment of existing RC buildings designed according to previous non-seismic codes and exposed to various levels of corrosion and mainshock-aftershock sequences. A refined finite element model of an existing four-storey reinforced concrete building is adopted. A selection of twenty as-recorded natural ground motions are collected from international database to perform incremental dynamic analyses for the inelastic response of the testbed building. The effects of corrosion are applied on external beams and columns as to simulate a realistic exposure. The robust fragility assessment is conducted for a range of seismic intensity measures. Moreover, a new intensity measure, based on the modified acceleration spectrum intensity, is proposed. Such seismic parameter accounts for the elongation period experienced by structures during earthquake events and appears to be more reliable and accurate for corroded RC structures than the most commonly adopted peak ground acceleration and spectral acceleration at the first natural period. The results of the comprehensive numerical simulations contribute to providing relevant indications on the non-linear response of existing corroded buildings under multiple excitations and, highlight that current seismic codes are no longer conservative for such detrimental phenomena.

Keywords: Corrosion; ageing effects; mainshock and aftershocks; reinforced concrete structures; smooth bars; inelastic response.

1. Introduction

Many existing and newly reinforced concrete (RC) structures in seismic prone countries are designed to withstand single strong ground motions. However, the complexity of fault systems and the dynamic stresses generated by single events may trigger multiple aftershocks (Ruiz Garcia et al., 2012). Potentially, aftershocks may be either comparable or stronger than mainshocks. Due to the short time of occurrence after mainshocks, such aftershocks could completely change the inelastic response of RC structures and cause collapse.

Some existing studies have focused on the effects of earthquake swarms on the non-linear response of single-degree-of-freedom (SDOF) (i.e. Amadio et al., 2003; Hatzigeorgeiou and Beskos, 2009; Sabegh and Ruiz Garcia, 2015). They investigated the effects of the earthquake sequences on q-factor and ductility of SDOF systems. The results of the numerical analyses indicated that the large damage accumulation due to mainshock-aftershock sequences implies a strong decay of the q-factor and an increasing demand in the inelastic displacement ratio, which depend on some parameters of the SDOF system and local site conditions such as structural period, available ductility, damping ratio and the type of the earthquake ground motion and soil. Conversely, some other researchers focused on the inelastic response of multiple-degree-of-freedom (MDOF) subjected to multiple ground motions (Li and Ellingwood, 2007; Hatzigeorgiou and Liolios 2010; Di Sarno, 2013; Hosseinpour et al., 2017, Aldenaby, 2018). On the one hand, Li and Ellingwood (2007) investigated the effects of sequential ground motions on steel moment frames and proposed a new methodology to incorporate the additional damage due to aftershocks in the performance-based assessment. On the other hand, Di Sarno (2013), Hatzigeorgiou and Liolios (2010), Hosseinpour et al., (2017), Aldenaby, (2018) carried out numerical simulations on the effects of such multiple earthquakes on RC framed structures. Moreover, a fragility assessment was also presented in Hosseinpour et al., (2017) and Aldenaby, (2018). The results of these comprehensive analyses led to either an increase in the inelastic displacement or even a collapse of RC frames, in comparison to an elastic or slightly inelastic behaviour of single ground motion-subjected structures. The fragility analysis highlighted the significant impact on the increasing failure probability of RC frames under multiple earthquakes. The accumulation of plastic deformation due to the short time of occurrence between two events showed an increment of inter-storey drift ratios and the incapability of such structures to redistribute the internal forces. All these studies suggest that an adequate and accurate hysteretic model, accounting for strength and stiffness degradation, should be considered in order to reliably predict the non-linear response of RC structures under such earthquake sequences.

Most of these studies on the non-linear behaviour of RC structures under motion sequences have utilized replicated or artificial aftershocks. However, such an approach may lead to unreliable results as aftershocks contain different characteristics from mainshocks, even if they occurred in the same region. Furthermore, those numerical simulations have been conducted mostly on two-dimensional models without any consideration for the interaction between frames and connections, and the possible exposure of such RC structures to aggressive environments, which may foster further damage and deterioration due to corrosion.

Corrosion has a destructive and extensive impact on RC civil infrastructure (Panchireddi et al., 2018; Ma et al., 2020, Guo et al., 2020; Di Sarno and Pugliese, 2020a, Di Sarno and Pugliese, 2020b).

Concrete and steel reinforcement are affected by corrosion differently. While concrete cover spalling and the reduction of the compressive strength are the main consequences for concrete (i.e. Coronelli and Gambarova, 2004), mass loss and reduction of mechanical properties are the corrosion effects for steel reinforcements (i.e. Cairns et al., 2005, Apostolopoulos et al. 2006, Imperatore et al., 2017). Additionally, high corrosion rates weaken the bond strength between the concrete and rebars (i.e. Almusallam et al., 1996; Bilcik and Holly, 2013; Coccia et al, 2016; Zhang et al. 2020) which may trigger the inelastic buckling. The effects of such inelastic instability for steel longitudinal bars lower the ultimate capacity of RC members and, thus, impact the global behaviour of the structure.

Although, corrosion is difficult to model and simulate due to its unpredictable nature and complexity, it is, however, essential to provide guidelines for the assessment of the inelastic response of typical existing RC buildings when subjected to multiple earthquakes and corrosion.

Many studies have dealt with the effects of corrosion on (RC bridges) unprotected structures (i.e. Gardoni et al., 2012; Ghosh and Sood, 2016, Shekhar et al., 2018) where the corrosion penetration could be included on the whole RC component. However, this scenario does not represent the real case of typical RC buildings as frames are protected by infills, and the corrosion path could stop on just one side. Only external RC components can be reasonably exposed to aggressive agents, leading to either a one- or two-sided attacks.

For this purpose, this study investigates the seismic vulnerability of typical existing RC buildings under multiple earthquake excitations and various levels of corrosion rates. Firstly, a selection of twenty ground motions were collected from international database. Then, a description of the finite element (FE) model of the RC building, along with the calibration of the mesh size density of RC components through moment-curvature analysis, is provided. A brief introduction on the pitting corrosion model and seismic fragility assessment is also presented. A new formulated intensity measure for fragility assessment, named Modified Acceleration Spectrum Intensity (MASI), is introduced. Such seismic parameter was assessed using some criteria from the literature. Then, the seismic fragility curves of the corroded building for three limit states and three seismic intensity measures, through incremental dynamic analysis (IDA), are given. Finally, based on the numerical results, conclusion and suggestions for future works are provided.

2. Research Significance

The research objectives of the present study are as follows:

- *Inelastic response of actual corroded RC buildings*: Incremental dynamic analyses will provide a relevant indication on the seismic response of existing RC buildings when exposed to corrosion and subjected to multiple earthquake loadings;

- *IDA analyses on a refined three-dimensional finite element model*: Previous research has primarily focused on a two-dimensional approach, while this study simulates the response of a three-dimensional model of a multi-storey residential building;
- *Seismic fragility analysis*: A probabilistic approach is herein used to evaluate the seismic vulnerability of a corroded 4-storey RC building considering three limit states, including Limited Damage, Severe Damage and Near Collapse. Structural performance points were taken as an average from non-linear static analyses using three different lateral loading patterns;
- *Evaluation of the adequacy of different intensity measure*. Three different parameters were used as IM: (i) peak ground acceleration, (ii) spectral acceleration for the first natural frequency of the building and (iii) Modified Acceleration Spectrum Intensity including the elongation period experienced by RC structures during the occurrence of earthquake events. The last two seismic intensity measures account for the elastic period of the corroded building. While the maximum inter-storey drift ratios were used as an engineering demand parameter (EDP)

3. GROUND MOTION SELECTION

In seismic-design, earthquake excitations are selected with regard to the site and structure specifications which require the response spectrum of natural records matching the target site response spectrum. Modern seismic codes specify that at least seven couples of ground motions should be considered to attain the mean inelastic response of RC structures (i.e. Eurocode 8 – Part 3, 2004). A set of twenty natural as-recorded ground motions were collected from international databases (PEER NGA strong motion database) and employed in the FE model. Each earthquake sample consisted of two horizontal components (X and Y, global axes) to simulate a far-field condition (epicentral distance – $R \geq 20$km). Table 1 provides the seismological parameters of the selected ground motion excitations. A time gap between mainshocks and aftershocks is assumed equal to thirty times the first fundamental frequency of the building to bring the structure to the rest and cease any movement caused by damping (Figure 1).

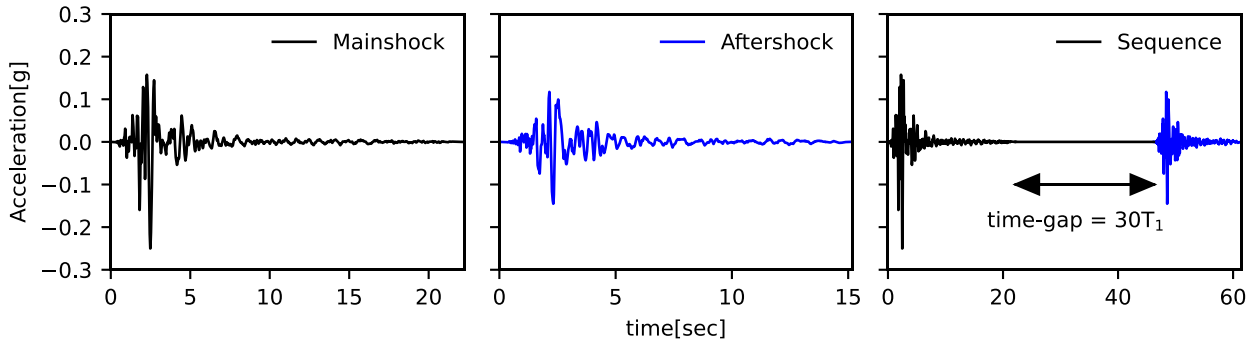

Figure 1. An example of the mainshock, aftershock and earthquake sequence used in this study

The statistical correlation of significant duration (X and Y) and predominant period (X and Y) for mainshock and aftershock ground motion pairs was investigated and depicted in Figures 2 (Song et al., 2014). Aftershocks were found mildly correlated to their mainshock counterpart for the significant duration and weakly correlated for the predominant period.

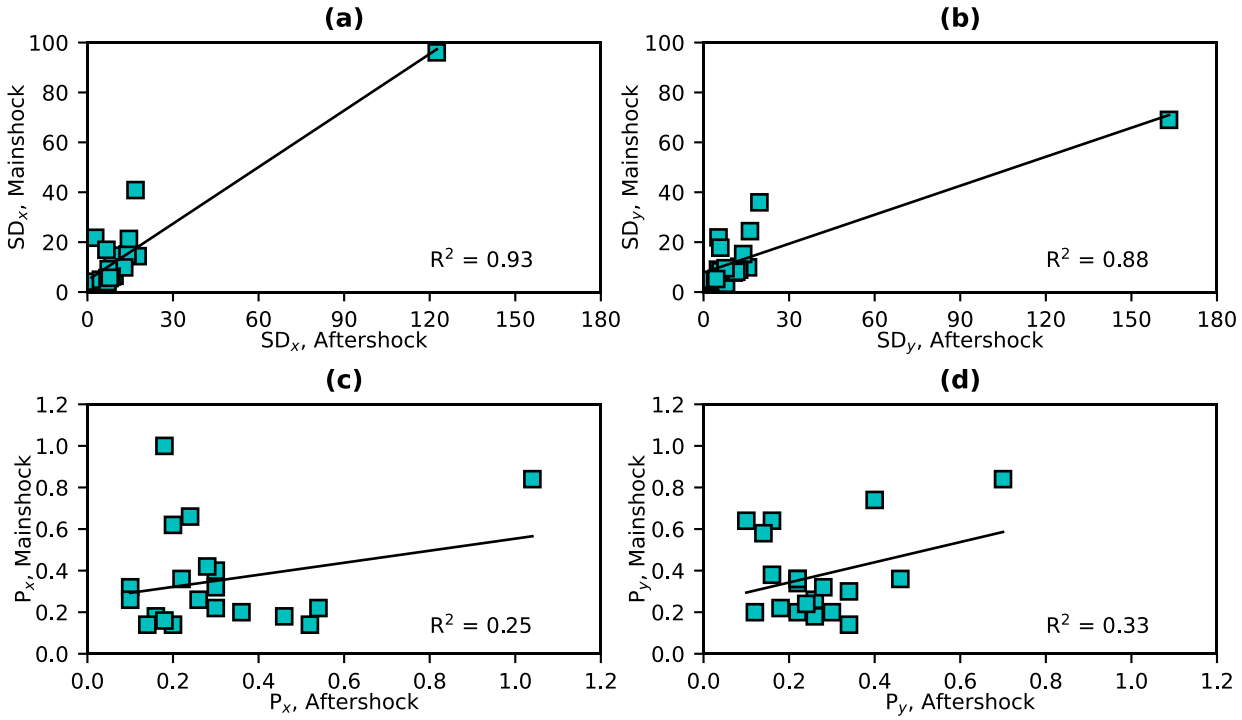

Figure 2. Correlation between mainshocks and aftershocks: (a) Significant Duration along X; (b) Significant Duration along Y; (c) Predominant Period along X and (d) Predominant Period along Y

4. RC BUILDING MODEL

An existing four-storey RC building was used as testbed and implemented in an advanced FE software (Seismostruct, 2018). Cross-sections of columns were 350x350 mm^2 for the ground floor and

300x300 mm^2 for the remaining floors, reinforced with 6-Φ16mm longitudinal rebars and Φ6mm transverse stirrups with 150mm spacing. The beams had different cross-sections (edged beams 300x500 mm^2, internal beams 800x200 mm^2), mainly reinforced with Φ14- Φ10 longitudinal bars and Φ6 transverse rebars with 200mm spacing. The initial compressive strength of the concrete and yielding stress of steel reinforcement were taken equal to 20 MPa and 440 MPa, respectively, according to original design specifications and some studies from the literature for existing RC buildings built in Italy between the 60s and 70s (i.e. Verderame et al., 2010; De Luca and Verderame, 2013; Manfredi et al., 2014). Then, a confidence factor of 1.2 was applied due to the uncertainties and incomplete information for materials and geometry. Both columns and beams were discretized into small fibres for the cross-sectional response, using various degrees of mesh density and defined with proper stress-strain relationships. To adequately predict the response of RC columns and beams, accurate models for concrete (cover and core) and steel reinforcements should be considered. Chang-Mander (1989) and Monti-Nuti (1992) constitutive material models for concrete and steel reinforcement were herein used (Figures 3). Such materials have been numerically identified to accurately simulate the seismic response of un-corroded and corroded RC components (Di Sarno and Pugliese, 2019 and 2020a).

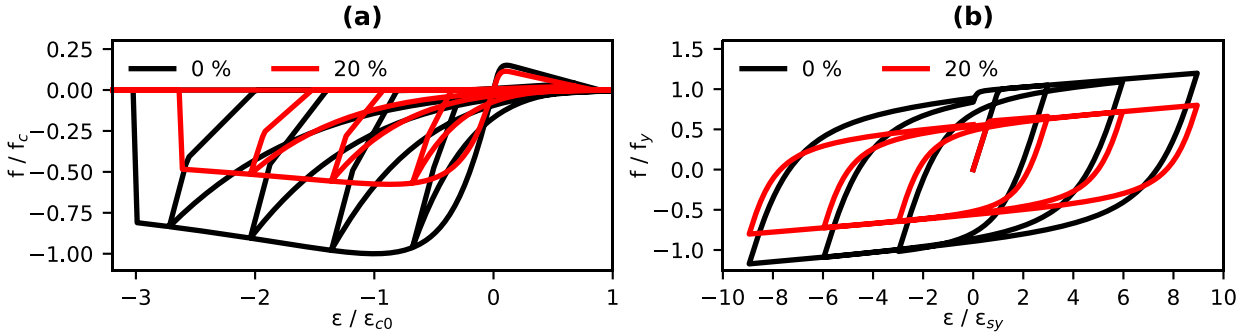

Figure 3. Example of un-corroded and corroded constitutive material model: (a) Concrete Chang-Mander (1989) and (b) Steel Monti-Nuti (1992)

The well-known and documented distributed-plasticity through force-based elements with five integration points was adopted (Spacone et al., 1996, Part I and Part II), both for columns and beams. Yet, the accuracy and reliability of the cross-sectional response of columns and beams strongly depend upon the mesh density of the core and cover concrete. Thus, a calibration of such mesh size was needed to find the best trade-off between efficiency and minimal computational cost demand. A range of fibers between 100-to-400 was chosen to calculate the moment-curvature of a two-dimensional inelastic force-based element implemented in the software. The numerical results were validated against the moment-curvature generated by the analysis open-source program

Response2000 (Bentz and Collins, 2001) developed at the University of Toronto and shown in Figures 4. Moreover, the area predicted (from the numerical analysis) over the area measured (from Response2000) through the trapezoidal rule and the computational time were plotted versus the numbers of discretized fibers in Figure 4b and 4c (users can choose the number of discretization points (n_{dp}), but the software will automatically divided the fibers for core and cover concrete as for a non-uniform discretization).

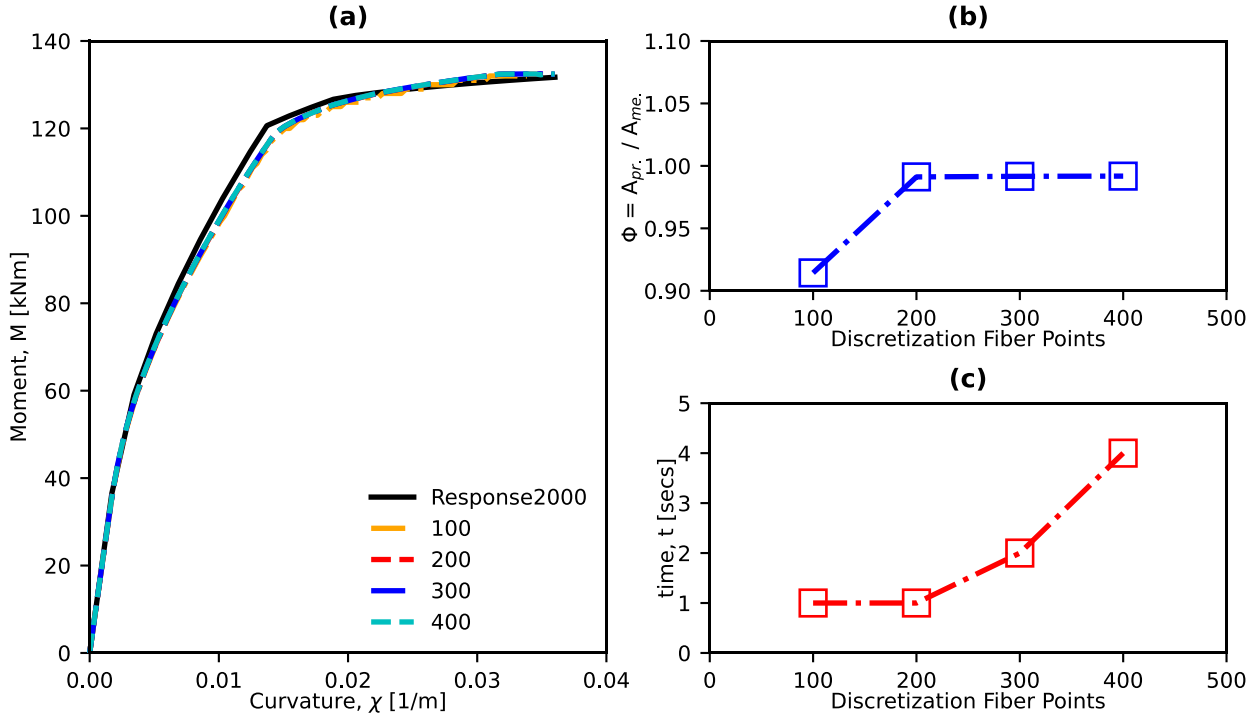

Figure 4. Moment-Curvature (M-χ) validation model in Seismostuct: (a) M-χ comparison with different discretization schemes; (b) Area predicted over area measured vs discretization schemes; (c) computational time cost demand vs discretization schemes

Outcomes showed that a number of fibers beyond 200 did not further improve the accuracy of the cross-sectional response (the ratio $\Phi = A_{predicted}/A_{measued}$ was almost equal to 1 for $n_{dp} \geq 200$), but rather doubled the computational time. Therefore, n_{dp} equal to 200 was the compromise between efficiency and numerical demand.

Rigid diaphragms were implemented to model slabs to ensure in-plane stiffness properties, while all the joints were connected through fully-supported-rigid-connections (all degrees of freedom were restrained) to the ground. A comprehensive and accurate loading analysis was conducted and applied to building model. The FE model view is given in Figure 5.

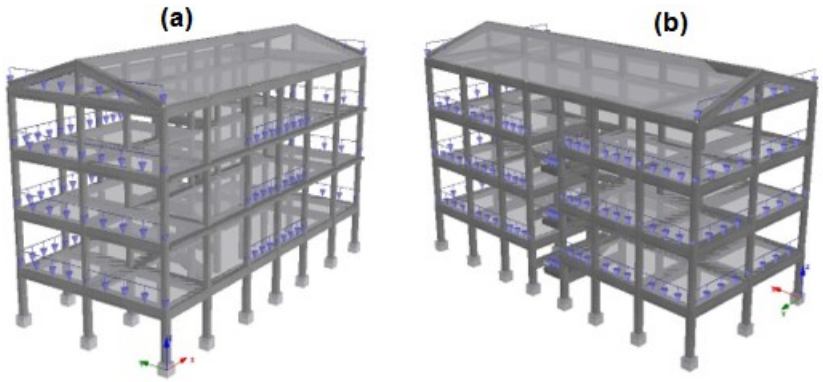

Figure 5. Finite model of the sample structure implemented in the finite element computer platform: (a) North and (b) South views

5. CORROSION MODELLING APPROACH

Typically, RC components are protected by infills which can produce either a one- or two-sided attack; as a result, corrosion was applied only to external beams and columns in order to simulate a realistic exposure (Figure 6).

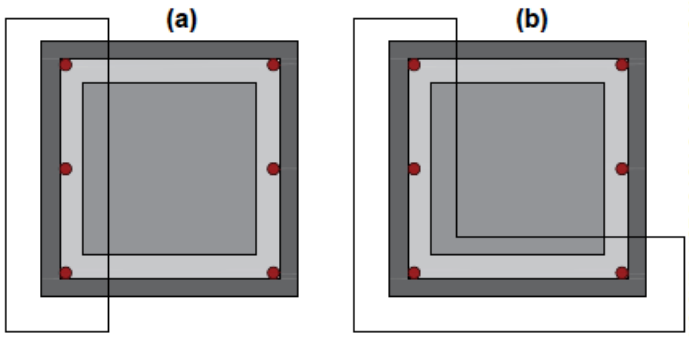

Figure 6. Typical 350x350 mm^2 RC column. (a) one-sided and (b) two-sided attack

Since the RC building is close to a marine environment, the presence of high chloride contents is likely to generate localized corrosion. Pitting corrosion is more detrimental than uniform corrosion and it is related to the depth of pits along the steel bar. Thus, the mass and diameter losses of steel reinforcement refer to the ratio between the maximum pit depth and the mean of such pits along the bar (pitting factor – R), which can be expressed as follows:

$$R = \frac{X_{max}}{X_{mean}} \quad (1)$$

The maximum penetration (X_{max}) of pitting corrosion is about four-to-eight times the average penetration (uniform corrosion) on the steel rebars (Gonzales et al., 1995). Moreover, Yu et al. (2015) carried out an experimental investigation to study the corrosion distribution of steel bars of RC beams exposed to natural corrosion. They found that the pitting factor (R) ranged between 2.5 and 5.0; however, the measured maximum depth of the corrosion penetration was equal to five over an average cross-sectional loss of 5-to-20%. Thus, a pitting factor of 5 was assumed in this study.

The corrosion reinforcement ratio (CR [%]) in terms of area loss was expressed as:

$$\mathrm{CR}[\%] = \frac{\mathrm{A_0} - \mathrm{A_p}}{\mathrm{A_0}} \times 100 \qquad (2)$$

where A_0 is the area of the un-corroded steel bar, and A_p is the net cross-sectional area of the corroded rebar. The model proposed by Rodriguez et al. (1997) was used to estimate the residual cross-section area of steel bars. Hence, the compressive strength of the concrete and the mechanical properties of steel reinforcement, in terms of strength and ductility, were modified according to Di Sarno and Pugliese (2019 and 2020a). Figure 7 depicts the prediction of the residual capacity of the corroded (one-side and two-side) RC cross-section according to the above-mentioned model.

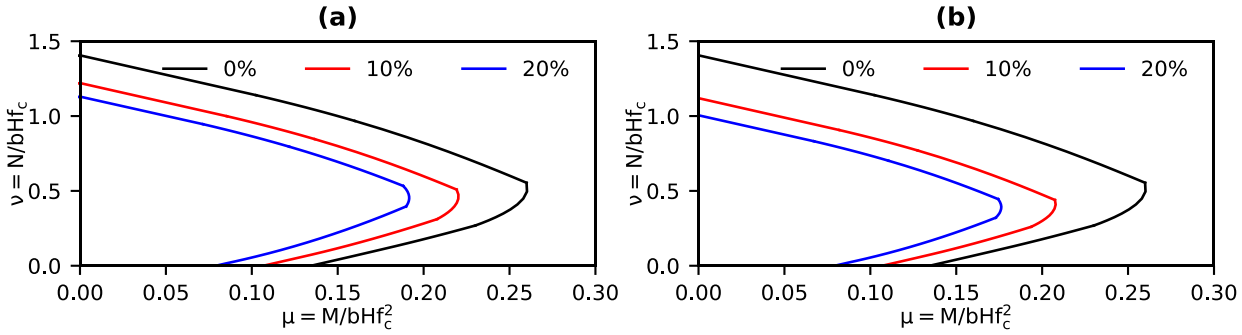

Figure 7. Interaction surface axial load-bending moment: (a) one-sided attack; (b) two-sided attack

The main aspects in the structural modelling, such as the evolution and the reduction of the geometry and material properties due to the effects of corrosion can be summarized, as follows (Figure 8):

- Reduction of steel rebars area using the Rodriguez's model;
- Change in the yielding and ultimate strength of the steel reinforcement;
- Change in the ductility (reduction of the ultimate strain) of steel rebars;
- Reduction of the strength and ductility of the concrete cover and core. (Concrete cracking is associated with the strain at the peak of compressive strength and taken as $\boldsymbol{\varepsilon_{c0} = f_c^{0.25}/1100}$ (Chang and Mander, 1989). It decreases with the reduction of the concrete compressive strength. The value of the ultimate strain is taken three times $\boldsymbol{\varepsilon_{c0}}$ (Chang and Mander, 1989),

and reduced accordingly. Once spalling of cover concrete occurs, this layer does not contribute any longer to the response of the RC component);

- Reduction of the flexural stiffness of RC components ($\mathbf{E_c = 8200 f_c^{0.375}}$, decreases according to the reduction of the concrete compressive strength);

Further details on the constitutive models of steel reinforcement and concrete, and the seismic response of RC columns subjected to corrosion effects can be found in Di Sarno and Pugliese (2020a).

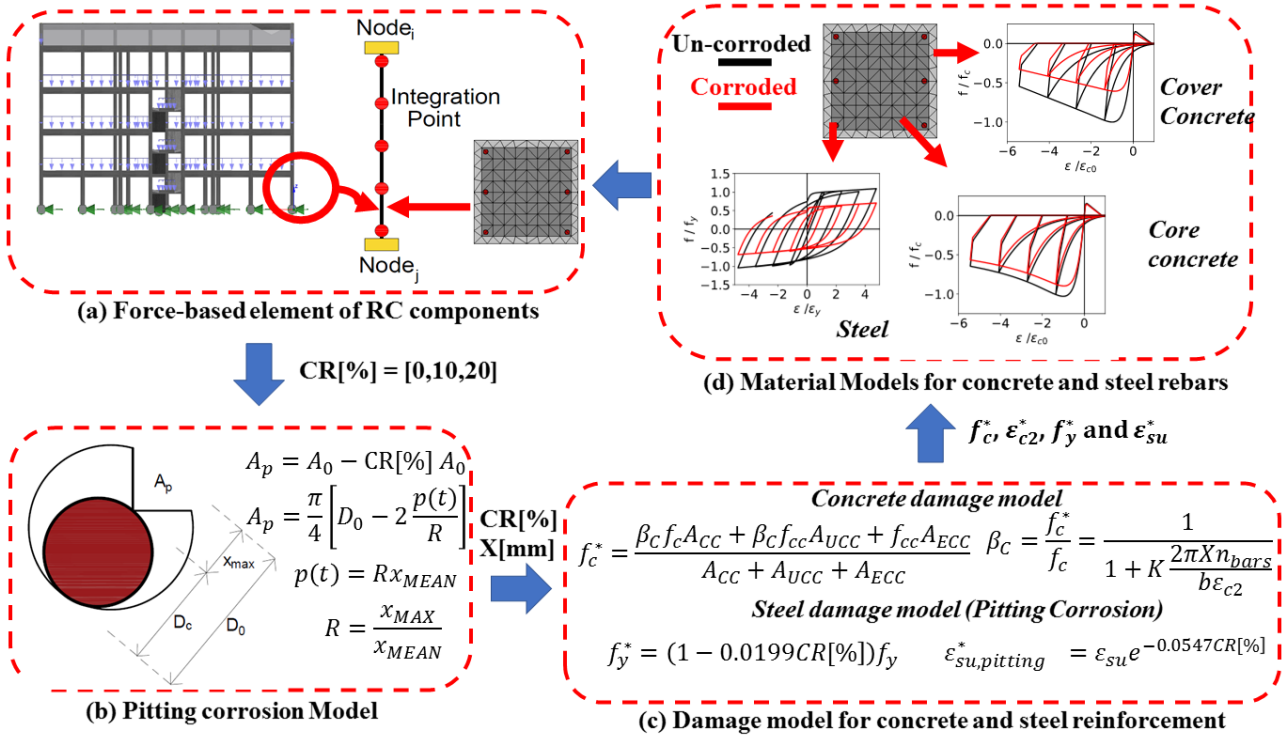

Figure 8. Simulation procedure of pitting corrosion

6. SEISMIC FRAGILITY EVALUATION

The inelastic response of the existing RC building was evaluated through the IDA procedure (Vamvatsikos and Cornell, 2002). The structure was subjected to three different earthquake excitations, i.e. (a) mainshock, (b) aftershock and (c) mainshock-aftershock sequence, and various levels of corrosion rates, i.e. CR [%] = 0%,10%, and 20%.

The set of ground motions were adequately scaled to simulate the linear and nonlinear response of the RC building using the hunt-fill algorithm (Vamvatsikos and Cornell, 2004). This method was used to (a) pick an initial elastic brunch (e.g. PGA = 0.005g) with six steps until the first non-convergence issue was obtained in terms of infinite value of the inter-storey displacement, and (b) the inelastic response ("flatline") with two additional steps. Such additional scaling-coefficients referred to either the structure collapse or large inter-storey drift ratios. A typical relationship between damage measure quantity (engineering demand parameter - EDP) and intensity measure (IM) was

then obtained by interpolation. EDP was herein related to the maximum inter-storey displacement (ϑ_{MAX}). Then, the seismic fragility analysis was carried out.

The seismic probability risk assessment method is the most widely adopted approach for the evaluation of the global and local response of RC structures. Such seismic vulnerability assessment requires the definition of a specific limit to obtain the probability of exceedance by using the following relationship (3):

$$P(EDP_i \geq EDP_{LS} | IM = x) = \Phi\left[\frac{1}{\beta_i} \ln\left(\frac{IM}{LS_i}\right)\right] \quad (3)$$

where P is the probability of exceedance of the specified limit state based on ground motion intensity, Φ is the probability density function of a normal distribution, β_i is the lognormal standard deviation, and LS_i is the median value that represented a ground motion intensity that has 50% probability for the occurrence of the defined limit state.

Three limit states were explicitly adopted in this study such as limited damage (LD), significant damage (SD) and near collapse (NC). Such structural limits were identified by performing nonlinear static analyses on the existing RC building, in both global directions X and Y, including three different lateral loading patterns (the mean values were obtained using the square root of sum of squares - SRSS) and the examined levels of corrosion. The maximum inter-storey drift ratio (MIDR) threshold values are shown in Table 2. Further details on the definition of the performance points can be found in the study of Di Sarno and Pugliese (2020a).

Table 1. Limit States expressed as inter-storey drift ratio, IDR [%]

Corrosion Rate - CR [%]	NC [%]	SD [%]	LD [%]
0	2.30	1.87	1.06
10	1.69	1.44	0.93
20	1.21	1.17	0.90

(*Keynote*: NC = Near Collapse; SD = Severe Damage; LD = Limited Damage).

7. SEISMIC INTENSITY MEASURE

The probabilistic approach for the evaluation of the seismic vulnerability of RC structures is related to an appropriate estimation of the seismic intensity measure that leads to an adequate characterization of the relationship between the earthquake excitation features and the inelastic behaviour of RC structures. Since IM is capable of quantitatively affecting the seismic response, a proper choice should be then carried out. This study investigates three different IMs: (a) peak ground acceleration (PGA), (b) spectral acceleration at the first natural period of the building ($Sa[T_1]$), and the modified

acceleration spectrum intensity (MASI) that accounts for the elongation period of the structure during an earthquake occurrence.

PGA is the most widely adopted parameter for engineering applications as it is explicitly related to the inertia forces that appear in structures. Although widely used, it has been criticized for its weak correlation with ϑ_{MAX}. Thus, it is often challenging to obtain a reasonable fitting. An overestimation, in fact, of the structural seismic vulnerability may occur as a result of this weak correlation. S_a is the spectral acceleration that represents a measure of what the structure experiences during an earthquake, while $S_a[T_1]$ is the spectral acceleration concerning the first natural period of the structure. The last parameter is commonly used because of its accurate fitting with the EDP and for its adequate correlation with ground motion and building information. As a result, modal analyses were performed for each level of corrosion and T_1 used for computing the spectral acceleration. MASI is the modified acceleration spectrum intensity. Such seismic IM requires the definition of two periods of vibration of an RC structure. Typically, strong ground motions force the structures to elongate their natural periods and, thus, a direct measure of the inelastic response of the building and the associated damage. Although laborious to estimate, Eurocode 8 (EN 1998 – Part-3, 2004) states that the maximum elongation period due to the non-linear behaviour is twice the fundamental period of the structure, which is reasonable for existing non-seismic designed structures. It can be defined as follows:

$$\mathrm{MASI} = \int_{T_1}^{2T_1} S_a(T)\,dT \tag{4}$$

To find out whether or not an IM is optimal, some researchers (e.g. Mackie et al., 2001; Cornell et al., 2002; Giovenale et al., 2004; Luco et al.,2007; Padgett et al., 2008, among others) proposed feasible criteria such as efficiency, sufficiency, practicality, proficiency and hazard computability. The efficiency criterion refers to the dispersion of the seismic demand, that is the logarithmic standard deviation ($\sigma_{\log\eta|IM}$) of the pair EDP-IM. Low values of $\sigma_{\log\eta|IM}$ results in less dispersion of EDP-IM interpolation.

$$E\left[\left(\frac{\theta_{MAX}}{\theta_{LSi}}\middle|IM_i\right)\right] = \log\eta|IM = \log a + b\log IM \tag{5}$$

$$\sigma_{\log\eta|IM} = \sqrt{\frac{\sum_{i=1}^{n}\left(\log\frac{\theta_{MAX}}{\theta_{LSi}} - \log\eta|IM\right)^2}{n-2}} \tag{6}$$

311 Practicality is associated with the dependency of the intensity measure to the seismic demand. Such
312 IM refers to the slope of the fitting curve (b in eq. 5). The larger the values of the slope, the more
313 practical the IM is. Proficiency was introduced by Padgett et al. (2008), and it is an explicit measure
314 for balancing the efficiency and practicality. It is defined as the ratio between the logarithmic standard
315 deviation of the seismic demand and the slope of the fitting curve. Small values of this ratio imply
316 higher proficiency for IM ($\psi = \sigma_{\log\eta|IM}/b$). Finally, the sufficiency is a measure of the statistical
317 independence from the ground motion parameters (e.g. magnitude). The sufficiency can be estimated
318 through the slope of the linear regression between the residuals (EDP-IMs) and magnitude of the
319 selected ground motions. The smaller the slope, the higher the sufficiency.
320 To obtain the relationship between EDP and IM for the entire the case-studies (mainshock, aftershock
321 and mainshock-aftershock sequence), the set of twenty ground motions were employed in the FE
322 model in both global directions (X and Y), while the SRSS was used to combine those parameters.
323 The values of ϑ_{MAX} obtained from the numerical analysis were normalized with respect to the limit
324 state of SD. However, it can be demonstrated that each limit state leads to the same result.
325 Evaluation of the optimal IM for the case-study RC building was conducted using the three
326 earthquake scenarios (aftershock, mainshock, and mainshock-aftershock sequence motions) and
327 shown in Figures 9, 10 and 11. As illustrated in the figures, MASI appeared to be the most efficient
328 IM as it allows to obtain a reduced variability in the structural response due to its lowest value of the
329 standard error compared to the other examined IMs. The high efficiency of MASI could probably lie
330 in the relevant inelastic effects of higher modes included in the period range $T_1 - 2T_1$ that allowed to
331 capture the degree of non-linearity of the structural response. The last finding was also observed when
332 corrosion increased. Similar results were obtained for $Sa(T_1)$ which exhibited a slight increase in the
333 standard error when the building was subjected to the effects of corrosion. Such a gap disappeared
334 for the seismic sequence (mainshock-aftershock), possibly due to the damage accumulation and larger
335 natural frequencies (beyond $2T_1$) experienced from the structure during the occurrence of the multiple
336 excitation, which was not included in the evaluation of MASI. Conversely, the highest dispersion
337 exhibited by PGA demonstrated its poor effectiveness to measure the damage potential for RC
338 structures.
339 Instead, large values of the slope of the data interpolation line allowed to recognize the high
340 practicality of all IMs, even when the RC building was under earthquake sequences and increasing
341 level of corrosion, which implied a strong correlation of such seismic intensity parameters with the
342 engineering demand by means of the inter-storey displacement.
343 Moreover, Figures 9, 10 and 11 show that MASI was the most proficient IM considering the entire
344 earthquake and corrosion case-studies. The last finding indicates that such a seismic parameter needs

reduced number of non-linear analyses to estimate the seismic vulnerability of a corroded and uncorroded RC structure under various earthquake condition while reducing the uncertainty into the model analysis.

Figures 12 depict the evaluation of the sufficiency for the investigated IMs. The results illustrate that PGA is strongly correlated to the earthquake features because of its highest slope of the fitting curve. On the other hand, MASI seemed to be completely independent from the earthquake characteristics with the approximately zero slope of the linear interpolation. This last observation could be confirmed by the structural information parameters included in the evaluation of such IM, which is reliable and accurate even when the building is subjected to detrimental effects (i.e. pitting corrosion)

8. SEISMIC FRAGILITY ANALYSIS

The damage analysis is herein used to estimate the probability of failure for specific limit states. Such failure probability is investigated at both components and global systems as a function of the inelastic response, and for a given intensity measure. The statistical approach used for this type of analyses, which correlates the demand and the capacity, is the "fragility analysis". Three limit states are discussed hereafter: (a) Limited Damage – LD, (b) Severe or Significant Damage – SD, and (c) Near Collapse – (NC).

8.1 LIMITED DAMAGE

Current seismic regulations commonly account for single strong ground motions to evaluate the seismic response of RC structures; as a result, earthquake sequences and corrosion are often neglected. However, such detrimental phenomena could cause additional damage and deterioration that may lead to an overprediction of the actual response of existing RC buildings if those stated threshold limits (EN 1998 – Part-3, 2004) are being used. Therefore, the fragility curves were built using both the limit states from technical codes (i.e. d/H = 1% for the limit state of LD; EC in Figures) and non-linear static pushover analyses (i.e. Table 2; SPO in Figures).

Figures 13 show the fragility curves and the difference in the failure probability of the RC building subjected to aftershock motions and various levels of corrosion. Although the limit state of LD occurred for low-scaled ground motions, results from the numerical simulations showed a significant reduction of the seismic capacity and a relevant increase in the failure probability of the corroded RC building. For the limit state of SPOs, the RC building with CR=10% exhibited the maximum increase in the probability of exceedance of 27.4% at a PGA of 0.251g, whereas for CR=20% the failure probability showed an increment of 27.2% at a PGA of 0.241g. On the contrary, it produced an

increase in the fragility equal to 20.2% and 23.2% at PGAs of 0.260g and 0.241g, respectively, for the limit state posed by Eurocode 8 (EN 1998 – Part-3, 2004). A more relevant impact of corrosion was instead observed for the IMs of MASI and Sa(T1). On the one hand, the probability of exceedance using the SPO limits ranged between 56.7% and 67.2% for the examined corrosion rates at almost the same Sa(T1) (0.240g), compared to 45.8% and 54.8% obtained from EC limits at a Sa(T1) of 0.235g. On the other hand, MASI demonstrated an increase in the failure probability by 45.1% and 53.7% for CR=10% and 20%, respectively, in contrast to the smaller values of 34.5% and 41.1% for the current technical codes.

Figures 14 and 15 show the seismic fragility assessment for the RC building subjected to mainshock and sequence motions. Compared to aftershock motions, mainshock and earthquake sequences produced larger inter-storey displacements and an increase in the structural vulnerability. The last observations can be explained by stronger and longer (in duration) ground motions and additional damage produced by multiple earthquakes.

It can be observed in Figures 14 that the corroded RC building (CR=20%) under mainshock motions exhibited the maximum increment in the failure probability of 66% and 71.5% for the IMs of MASI and Sa(T1), respectively, while PGA produced a more conservative increase (41.8%). Unlike mainshock earthquakes, the effects of sequential motions exposed the structure to larger inter-storey drift ratios and a faster redistribution of the seismic forces due to the short time of occurrence between the mainshock and the aftershock. The above implied further damage and an increase in the vulnerability of the RC structure, about 85.9% for the modified ASI and Sa(T1), and 45.6% for the PGA, which led to an increment 17% in contrast to the mainshock case-study. In addition, the fragility curves, both for mainshocks and multiple earthquakes, for the threshold limit stated in the Eurocode 8 (EN 1998 – Part-3, 2004) were investigated. Such fragility curves yielded slightly more conservative failure probabilities as opposed to those obtained using the limits from the non-linear static pushover of the corroded building (Black lines in Figures 14 and 15). The last finding can be explained by similar values of the threshold limits stated in the Eurocode 8 (EN 1998 – Part-3, 2004) and those obtained from the non-linear static analyses.

Finally, the comparison of the fragility curves for each case-study ground motion demonstrated that the damage associated with the seismic sequences almost doubled the failure probability of the RC structure for each IMs compared to the aftershock and mainshock scenarios.

8.2 SEVERE DAMAGE

The limit state of severe damage (SD) usually occurs for high values of the scaled records when performing the IDAs, which implies more evident effects of corrosion due to the relevant decay of

410 both the structural stiffness and lateral strength. The threshold limit from the Eurocode 8 (EN 1998 –
411 Part-3, 2004) for the SD, in terms of inter-storey drift ratio, was herein taken equal to 2%.
412 Figures 16 show the fragility assessment conducted for the RC building subjected to aftershock
413 motions. Results from the numerical analyses demonstrated that the overall seismic fragility at the
414 system level increased as the RC building continued to corrode. For example, for a ground motion
415 with PGA = 0.4g, the probability that the pristine building could exceed the limit state of SD was
416 30%, in comparison with 75% and 85% with CR=10% and 20%, respectively. The maximum
417 increment in the failure probability was achieved at PGAs of 0.391g and 0.341g with a total increase
418 of 27.6% and 40.7 for the examined corrosion rates. Conversely, MASI and Sa produced completely
419 different results as opposed to those obtained by using the PGA as IM. Although showing similar
420 trends, the values of the failure probabilities over the corrosion rates of 10%-to-20% ranged between
421 47.6% and 66.6%, and between 59.7% and 79% for MASI and Sa(T1), respectively.
422 Moreover, it is worthy noticing that the maximum inter-storey drift ratio stated in the Eurocode 8 (EN
423 1998 – Part-3, 2004) generated more conservative failure probabilities, especially for the corroded
424 RC building. The last observation can be confirmed by the large difference between the two threshold
425 interval limits (SPO and EC) used in this study.
426 Figures 17 and 18 show instead the fragility curves of the RC structure exposed to mainshock and
427 earthquake sequences. Unlike the aftershock scenario, mainshocks and seismic sequences caused a
428 major reduction of the seismic capacity of the building and, thus, a large increase in the failure
429 probability. In comparison with MASI and PGA, the IM related to Sa(T1) provided the highest
430 increment in the seismic fragility when the RC structure was subjected to mainshock excitations.
431 Such failure probabilities were equal to 75% and 90% for CR=10% and 20%, respectively. Similar
432 results, in terms of seismic vulnerability increments, were obtained for MASI. Conversely, the RC
433 building with CR=10% exhibited a probability of exceedance of 44% at a PGA of 0.231g, whereas
434 for CR=20% the failure probability showed an increment of 60.6% at a PGA of 0.210g.
435 On the other hand, it is evident (Figured 18) that the damage accumulation induced by multiple
436 excitations caused a more extensive reduction of the seismic resistance of the RC building, compared
437 to mainshock and aftershock scenarios. The fragility assessment for the multiple earthquakes (Figure
438 18), indeed, led to a further increase in the failure probability of about 6.7% for the IMs of MASI and
439 Sa(T1), and 10% for the PGA, in contrast to the building subjected to mainshock excitations.
440 Finally, the fragility curves (black lines in the figures) obtained by using the threshold limits posed
441 by the Eurocode 8 (EN 1998 – Part-3, 2004) were plotted against the corrosion rates for all the
442 earthquake scenarios and depicted with black lines. The fragility analysis implied large conservative
443 results with almost 50% overprediction of the seismic vulnerability for each examined IM. The last

finding is a relevant indication of the lack of conservatism in the safety of non-seismic designed RC buildings exposed to various levels of corrosion and multiple earthquakes.

8.3 NEAR COLLPASE

The definition of the limit state of Near Collapse (NC) is always associated with large plastic deformations and strong inelastic behaviour of RC structures. Both the maximum inter-storey drift ratios from technical codes (4%) and non-linear static analyses (Table 2) were hereafter used to build the fragility curves.

Figure 19 shows the fragility assessment carried out for the testbed building subjected to aftershock motions. The outcomes obtained from the numerical simulations demonstrated that the seismic vulnerability increased over the corrosion rates for all the examined seismic IMs. For instance, for a ground motion having a PGA = 0.4g and the threshold limits from SPOs, there is 27% chance of achieving the collapse, while the values of 61% and 83% were obtained for the building with CR=10% and 20%. Conversely, the drift ratio from the Eurocode 8 (EN 1998 – Part-3, 2004) and for the same PGA, produced smaller failure probabilities, between 9.8% and 19.7% for the un-corroded and corroded building. Compared to the PGA, Sa(T1) and MASI induced a larger increase in the failure probabilities. Such values were equal to 85% at a Sa(T1) = 0.381g and 74.5% at a MASI = 0.161gs for the corrosion rate of 20% and the limits from Table 2. On the contrary, an overestimation of the seismic capacity could be observed for the fragility curves obtained using the limits from the Eurocode 8 (EN 1998 – Part-3, 2004).

Figures 20 instead illustrate the fragility assessment of the existing building subjected to mainshock motions. In comparison with aftershock case-study, mainshocks produced a larger increase in the seismic vulnerability of the testbed building. For example, the maximum increase in the failure probability was equal to 68% at a PGA = 0.231g, compared to 53% for the aftershock scenario. Instead, the values of 92.7% and 95% were observed for MASI and Sa(T1), which caused an increment of 23% and 11.7% in contrast with the structure subjected to aftershock motions. Such results were obtained performing fragility assessment with limits from non-linear static pushover analyses.

Unlike mainshocks, the effects of seismic sequences (Figures 21) almost doubled the seismic fragility of the structure when exposed to highly corrosive environments (i.e. CR= 20%). For example, a PGA equal to 0.231g produced a probability of exceedance equal to 75%, compared to 68% exhibited by the structure subjected to mainshock motions. On the contrary, both MASI and Sa(T1) showed similar trends with a total increase in the failure probability of 100% for the structure at a corrosion rate of

20%. Finally, the fragility curves computed by using the limit states from Eurocode 8 (EN 1998 – Part-3, 2004) led to smaller failure probabilities for each examined IM, which implied an overestimation of the real seismic capacity of the corroded building.

9. CONCLUSIONS

This analytical study contributes to providing a comprehensive framework for the performance of existing RC buildings under multiple excitations and various level of corrosion. The probabilistic fragility analysis was carried out to assess the seismic vulnerability of an existing four-storey RC building. A new seismic intensity measure based on the modified acceleration spectral intensity is presented. The proposed intensity measure accounts for the elongation period experienced by the structure during an earthquake event. The primary outcomes of the comprehensive numerical analyses can be summarised as follows:

- Results from the interpolation of the pair EDP-IM of un-scaled records based on the cloud method for assessing the efficiency, proficiency, practicality and sufficiency of the three IMs (i.e. PGA, Sa[T_1] and MASI), demonstrated that the newly formulated modified acceleration spectrum intensity, herein named MASI, appeared to be accurate and reliable for the evaluation of the seismic vulnerability of corroded RC structures. Such observations can be confirmed by low values of standard errors, high values of the slope of the power fitting line and small ratios between standard error and regression slope. Furthermore, the proposed intensity measure was also sufficient as it was un-correlated to the ground motion features, which is essential for the accuracy when performing fragility analysis;
- The effects of corrosion reduced the global seismic capacity of the testbed building and increased the failure probability for each examined limit states. PGA produced the lowest increments in the probability that the RC structure could exceed such threshold limits, compared to larger values obtained by using Sa(T1) and MASI. According to the numerical simulations, the seismic vulnerability was almost doubled (increment of 100%) when using the last two seismic intensity measures, especially when the building was subjected to mainshocks and earthquake sequences. This finding can be explained by the building information, such its natural frequencies, included in those seismic parameters;
- The damage and deterioration caused by multiple excitations induced larger inter-storey drift ratios compared to single strong ground motions. As a result, the building exhibited a further increase of the seismic vulnerability, i.e. 17% for the limit state of limited damage, in contrast with mainshock motions;

- The difference in the failure probability between CR=10% and 20% was small for the limit state of limited damaged in contrast with larger differences observed for the limit states of severe damage and near collapse. This was due to the achievement of the limited damage for low-scaled motions where corrosion produced similar effects on structural stiffness and strength;
- The fragility assessment using the limit states from non-linear static analyses contributed to indicating that current technical codes are longer conservative towards the safety of existing RC buildings exposed to multiple earthquakes and various levels of corrosion. Therefore, new provision should be provided in newly revised seismic technical codes to account for such detrimental phenomena;
- Additional investigations should also consider employing the uncertainties when analysing advanced and refined finite element models of RC structures. For instance, the probabilistic distributions of the main mechanical and geometrical properties of RC components (i.e. cover depth, position of longitudinal bars, stirrups spacing, diameter loss of steel rebars) should be included in the structural model.
- Future works should account for the time-dependency of the corrosion effects on RC buildings (i.e. statistical approach for time initiation and propagation). This allows the evaluation of the seismic vulnerability based on the lifetime of the structure rather than using the corrosion rate.

10. ACKNOWLEDGEMENTS

The authors would like to acknowledge the gracious support of this work through the EPSRC and ESRC Centre for Doctoral Training on Quantification and Management of Risk and Uncertainty in Complex Systems Environments Grant No. (EP/L015927/1).

Furthermore, the authors would also like to express their gratitude to the anonymous reviewers and Dr Raffaele De Risi, Lecturer at the University of Bristol (UK), who provided useful comments that have contributed to improving the quality of the manuscript.

11. REFERENCES

1. Abdelnaby, Adel E. (2018). Fragility Curves for RC Frames Subjected to Tohoku Mainshock-Aftershocks Sequences. *Journal of Earthquake Engineering*, Volume 22, Pages 902-920, Taylor & Francis, https://doi.org/10.1080/13632469.2016.1264328.
2. Almusallam AA, Al-Gahtani AS, Aziz AR and Rasheeduzzafar (1996) Effect of reinforcement corrosion on bond strength. Construction and Building Materials 10(2): 123-129.
3. Amadio, C., Fragiacomo, M., Rajgelj, S. (2003). The effects of repeated earthquake ground motions on the non-linear response of SDOF systems. *Earthquake Engineering and Structural Dynamics*, 32 (2), pp. 291-308.
4. Bentz E, Collins MP. Response-2000 user manual. Toronto, Canada: University of Toronto; 2001.
5. Cairns, J., Plizzari, G. A., Du, Y., Law, D. W., & Franzoni, C. (2005). Mechanical properties of corrosion-damaged reinforcement. *ACI Materials Journal*, 102(4), 256-264.
6. Ch.Alk. Apostolopoulos, M.P. Papadopoulos, Sp.G. Pantelakis (2006). Tensile behavior of corroded reinforcing steel bars BSt 500s, *Construction and Building Materials*, Volume 20, Issue 9, 2006, Pages 782-789, ISSN 0950-0618, https://doi.org/10.1016/j.conbuildmat.2005.01.065.
7. Chang, G.A., and Mander, J.B., (1994) "Seismic Energy Based Fatigue Damage Ananlysis of Bridge Columns:Part 1 – Evaluation of Seismic Capacity," *NCEER Technical Report No. NCEER-94-0006* State University of New York, Buffalo, N.Y.
8. Coccia, S., Imperatore, S. & Rinaldi, Z. Influence of corrosion on the bond strength of steel rebars in concrete. Mater Struct 49, 537–551 (2016). https://doi.org/10.1617/s11527-014-0518-x
9. Cornell, C. A., Jalayer, F., Hamburger, R. O., and Foutch, D. A. (2002). Probabilistic basis for 2000 SAC federal emergency management agency steel moment frame guidelines. *Journal of Structural Engineering, ASCE*, 128(4), pp. 526-533**.**
10. De Luca F. and Verderame G.M. (2013). A practice-oriented approach for the assessment of brittle failures in existing RC elements, Engineering Structures, 48:373-388.
11. Di Sarno L. and Pugliese F. (2019), Critical review of models for the assessment of the degradation of reinforced concrete structures exposed to corrosion, *Conference SECED 2019*, Earthquake Risk and Engineering towards a Resilient World. Doi: 10.6084/m9.figshare.12152778

12. Di Sarno, L. (2013), Effects of multiple earthquakes on inelastic structural response, Engineering Structures, Volume 56, 2013, Pages 673-681, ISSN 0141-0296. https://doi.org/10.1016/j.engstruct.2013.05.041.
13. Di Sarno, L., Pugliese, F (2020a). Numerical evaluation of the seismic performance of existing reinforced concrete buildings with corroded smooth rebars. *Bull Earthquake Eng* 18, 4227–4273 (2020). https://doi.org/10.1007/s10518-020-00854-8
14. Di Sarno, L., and Pugliese, F. (2020b). Seismic fragility of existing RC buildings with corroded bars under earthquake sequences, Soil Dynamics and Earthquake Engineering, Volume 134, 2020, 106169, ISSN 0267-7261, https://doi.org/10.1016/j.soildyn.2020.106169.
15. EN 1998-1, 2004. Eurocode 8: Design Of Structures For Earthquake Resistance. 1st ed. Brussels: BSi.
16. George D. Hatzigeorgiou, Asterios A. Liolios (2010). Nonlinear behaviour of RC frames under repeated strong ground motions, *Soil Dynamics and Earthquake Engineering*, Volume 30, Issue 10, Pages 1010-1025, ISSN 0267-7261, https://doi.org/10.1016/j.soildyn.2010.04.013.
17. George D. Hatzigeorgiou, Dimitri E. Beskos (2009). Inelastic displacement ratios for SDOF structures subjected to repeated earthquakes. *Engineering Structures*, Volume 31, Issue 11, Pages 2744-2755, ISSN 0141-0296, https://doi.org/10.1016/j.engstruct.2009.07.002.
18. Giovenale P, Cornell AC, Esteva L. Comparing the adequacy of alternative ground motion intensity measures for the estimation of structural responses. Earthquake Engineering and Structural Dynamics 2004; 33:951–979.
19. Gonzalez, J.A., Andrade, C., Alonso, C., & Feliu, S. (1995). Comparison of rates of general corrosion and maximum pitting penetration on concrete embedded steel reinforcement. Cement and Concrete Research, 25(2), 257–264.
20. Guo Z., Ma Y., Wang L., Zhang J. and Harik Issam E. (2020). Corrosion Fatigue Crack Propagation Mechanism of High-Strength Steel Bar in Various Environments. Journal of Materials in Civil Engineering, ASCE, Volume 32. doi: 10.1061/(ASCE)MT.1943-5533.0003165
21. Hosseinpour, F. & Abdelnaby, A.E.(2017). Fragility curves for RC frames under multiple earthquakes, *Soil Dynamics and Earthquake Engineering*, Volume 98, 2017, Pages 222-234, ISSN 0267-7261, https://doi.org/10.1016/j.soildyn.2017.04.013.
22. Imperatore, S., Rinaldi, Z. and Drago C. (2017), Degradation Relationships for the Mechanical Properties of Corroded Steel Rebars, Construction and Building Materials, Vol. 148, pg. 219-230.

608 23. Jayadipta Ghosh, Piyush Sood, Consideration of time-evolving capacity distributions and
609 improved degradation models for seismic fragility assessment of aging highway bridges,
610 Reliability Engineering & System Safety, Volume 154, 2016, Pages 197-218, ISSN 0951-
611 8320, https://doi.org/10.1016/j.ress.2016.06.001.
612 24. Juraj Bilcik, Ivan Holly, Effect of Reinforcement Corrosion on Bond Behaviour, Procedia
613 Engineering, Volume 65, 2013, Pages 248-253, ISSN 1877-7058,
614 https://doi.org/10.1016/j.proeng.2013.09.038.
615 25. Li, Q. & Ellingwood, B. R. (2007). Performance evaluation and damage assessment of steel
616 frame buildings under main shock–aftershock earthquake sequences. Earthquake Engineering
617 and Structural Dynamics, Volume 36 Issue 3, Pages 405-42. https://doi.org/10.1002/eqe.667.
618 26. Linwen Yu, Raoul François, Vu Hiep Dang, Valérie L'Hostis, Richard Gagné, Distribution
619 of corrosion and pitting factor of steel in corroded RC beams, Construction and Building
620 Materials, Volume 95, 2015, Pages 384-392, ISSN 0950-0618,
621 https://doi.org/10.1016/j.conbuildmat.2015.07.119.
622 27. Luco N, Cornell AC. Structure-specific scalar intensity measures for near-source and ordinary
623 earthquake ground motions. Earthquake Spectra 2007; 23:357–392.
624 28. Ma, Y., Guo, Z., Wang, L. and Zhang, J. (2020). Probabilistic Life Prediction for Reinforced
625 Concrete Structures Subjected to Seasonal Corrosion-Fatigue Damage. Journal of Structural
626 Engineering, ASCE, Volume 146, Issue 7, doi: 10.1061/(ASCE)ST.1943-541X.0002666
627 29. Mackie K, Stojadinovic B. Probabilistic seismic demand model for California bridges. Journal
628 of Bridge Engineering 2001; 6:468–480
629 30. Manfredi, G ., Prota, A., Verderame, G. M., De Luca, F., & Ricci, P.(2014). 2012 Emilia
630 earthquake, Italy: reinforced concrete buildings response. Bulletin of Earthquake Engineering,
631 12(5), 2275-2298.https://doi.org/10.1007/s10518-013-9512-x
632 31. Monti G., Nuti C. [1992] "Nonlinear cyclic behaviour of reinforcing bars including buckling,"
633 Journal of Structural Engineering, Vol. 118, No. 12, pp. 3268-3284.
634 32. NTC (2008): Approvazione delle nuove norme tecniche per le costruzioni, Gazzetta Ufficiale
635 della Repubblica Italiana, n. 29 del 4 febbraio 2008 – Suppl. Ordinario n. 30,
636 http://www.cslp.it/cslp/index.php?option=com_docman&task=doc_download&gid=3269&I
637 temid=10 (in Italian).
638 33. Padgett, J.E., Nielson, B.G. and Des Roches, R. (2008), Selection of optimal intensity
639 measures in probabilistic seismic demand models of highway bridge portfolios. Earthquake
640 Engng. Struct. Dyn., 37: 711-725. doi:10.1002/eqe.782.

641 34. Panchireddi, B and Ghosh, Jayadipta (2019). Cumulative vulnerability assessment of highway
642 bridges considering corrosion deterioration and repeated earthquake events, Bulletin of
643 Earthquake Engineering, Volume 17, Pages 1603-1638, ISSN=1573-1456,
644 doi=10.1007/s10518-018-0509-3.
645 35. Ramesh Kumar, Paolo Gardoni, Modeling Structural Degradation of RC Bridge Columns
646 Subjected to Earthquakes and Their Fragility Estimates, Journal of Structural Engineering,
647 10.1061/(ASCE)ST.1943-541X.0000450, 138, 1, (42-51), (2012).
648 36. Rodriguez, J., Ortega, L.M., & Casal, J. (1997). Load carrying capacity of concrete structures
649 with corroded reinforcement. Construction and Building Materials, 11(4), 239–248.
650 37. Ruiqiang Song, Yue Li, John W. van de Lindt (2014). Impact of earthquake ground motion
651 characteristics on collapse risk of post-mainshock buildings considering aftershocks,
652 Engineering Structures, Volume 81, Pages 349-361, ISSN 0141-0296,
653 https://doi.org/10.1016/j.engstruct.2014.09.047.
654 38. Ruiz-García J. (2012). Mainshock-aftershock ground motion features and their influence in
655 building's seismic response, J. Earthq. Eng., 16(5): 719–737.
656 39. Ryu, H, Luco, N., Uma, S.R. & Liel, A.B. (2011). Developing fragilities for mainshock-
657 damaged structures through incremental dynamic analysis. Proceedings of the Ninth Pacific
658 Conference on Earthquake Engineering Building an Earthquake-Resilient Society 14-16
659 April, 2011, Auckland, New Zealand.
660 40. Saman Yaghmaei-Sabegh, Jorge Ruiz-García (2016). Nonlinear response analysis of SDOF
661 systems subjected to doublet earthquake ground motions: A case study on 2012 Varzaghan–
662 Ahar events. Engineering Structures, Volume 110, Pages 281-292, ISSN 0141-0296,
663 https://doi.org/10.1016/j.engstruct.2015.11.044.
664 41. SeismoStruct, FEM Software, SeismoSoft, Earthquake Engineering Software Solutions,
665 Piazza Castello 19, 27100 Pavia – Italy, info@seismosoft.com.
666 42. Shivang Shekhar, Jayadipta Ghosh & Jamie E. Padgett (2018) Seismic life-cycle cost analysis
667 of ageing highway bridges under chloride exposure conditions: modelling and
668 recommendations, Structure and Infrastructure Engineering, 14:7, 941-966, DOI:
669 10.1080/15732479.2018.1437639
670 43. Spacone E, Filippou FC, Taucer FF (1996). Fibre beam–column model for non-linear analysis
671 of R/C frames. Part I: Formulation. Earthq Eng Struct D 1996; 25:711–25.
672 44. Spacone E, Filippou FC, Taucer FF (1996). Fibre beam–column model for non-linear analysis
673 of R/C frames. Part II: Applications. Earthq Eng Struct D 1996; 25:727–42.

45. Vamvatsikos, D. and Cornell, C.A. (2002), Incremental dynamic analysis. Earthquake Engng. Struct. Dyn., 31: 491-514. doi:10.1002/eqe.141.
46. Vamvatsikos, D., & Cornell, C. A. (2004). Applied Incremental Dynamic Analysis. Earthquake Spectra, 20(2), 523–553. https://doi.org/10.1193/1.1737737.
47. Verderame G.M., Polese M., Mariniello C., Manfredi G. (2010). A simulated design procedure for the assessment of seismic capacity of existing reinforced concrete buildings, Advances in Engineering Software, 41:323–335.
48. Zhang B, Zhu H, Chen J, Yang O. Influence of specimen dimensions and reinforcement corrosion on bond performance of steel bars in concrete. Advances in Structural Engineering. 2020;23(9):1759-1771. doi:10.1177/1369433219900682

12. APPENDIX

List of Tables:

Table 1. Seismological parameters.

Table 2. Main Seismological Parameters

Earthquake	Date	Event type	PGA_x [g]	PGA_y [g]	SD_x [sec]	SD_y [sec]	IA_x [m/sec]	IA_y [m/sec]	P_x [sec]	P_y [sec]
Spitak, Armenia	07/12/1988	MS	0.20	0.18	7.90	10.15	0.31	0.24	0.22	0.34
		AS	0.08	0.04	9.24	12.54	0.06	0.02	0.54	0.22
Valparaiso,Chile	24/04/2017	MS	0.39	0.68	40.88	35.96	6.81	15.07	0.14	0.22
		AS	0.18	0.19	16.86	19.59	0.68	0.73	0.52	0.18
North-West, China	12/05/2008	MS	0.27	0.19	14.38	9.90	0.49	0.61	0.14	0.36
		AS	0.13	0.14	17.62	15.60	0.19	0.21	0.20	0.22
Kalamata, Greece	13/09/1986	MS	0.25	0.14	2.70	4.11	0.28	0.08	0.32	0.30
		AS	0.15	0.27	2.82	1.87	0.11	0.30	0.30	0.34
Chamoli, India	29/03/1999	MS	0.19	0.37	14.60	8.98	0.29	0.80	0.66	0.36
		AS	0.04	0.07	8.80	5.06	0.01	0.02	0.24	0.22
Varzaghan, Iran	11/08/2012	MS	0.45	0.36	5.58	8.28	1.45	0.80	0.18	0.18
		AS	0.51	0.54	6.97	5.95	1.65	1.88	0.16	0.26
Emilia, Italy	20/05/2012	MS	0.26	0.26	5.60	5.99	0.69	0.84	0.32	0.26
		AS	0.22	0.29	7.54	6.97	0.76	1.28	0.10	0.26
Friuli, Italy	11/09/1976	MS	0.34	0.30	4.14	4.93	0.79	1.21	0.26	0.64
		AS	0.12	0.08	1.46	2.20	0.03	0.01	0.10	0.10
Irpinia, Italy	23/11/1980	MS	0.25	0.36	15.08	15.24	1.19	1.39	0.36	0.20
		AS	0.07	0.08	14.06	13.90	0.07	0.07	0.22	0.22
Nocera Umbria, Italy	26/09/1997	MS	0.56	0.49	4.95	4.35	3.29	2.80	0.16	0.38
		AS	0.52	0.31	4.73	4.10	0.86	0.70	0.18	0.16
Fukushima, Japan	11/03/2011	MS	0.39	0.42	21.30	24.41	2.44	3.40	0.62	0.64
		AS	0.14	0.13	14.55	16.28	0.14	0.14	0.20	0.16
Niigata, Japan	16/06/1964	MS	0.41	0.54	96.08	69.02	2.43	3.51	0.26	0.32
		AS	0.55	0.53	122.47	163.19	2.66	3.47	0.26	0.28
Christchurch, New Zealand	22/02/2011	MS	0.22	0.18	4.00	3.33	0.22	0.17	1.00	0.58
		AS	0.17	0.16	7.05	7.89	0.20	0.13	0.18	0.14
Edgecumbe, New Zealand	02/03/1987	MS	0.32	0.50	6.47	7.79	1.67	1.91	0.40	0.36
		AS	0.08	0.11	9.50	10.60	0.09	0.11	0.30	0.46
Weber, New Zealand	13/05/1990	MS	0.15	0.19	9.88	8.98	0.17	0.23	0.18	0.20
		AS	0.20	0.26	12.90	12.49	0.38	0.43	0.46	0.30
Chi-Chi, Taiwan	21/09/1999	MS	0.95	0.91	21.76	21.89	9.31	6.97	0.84	0.84
		AS	0.47	0.22	2.73	5.25	1.80	0.43	1.04	0.70
Duzce, Turkey	12/11/1999	MS	0.30	0.30	16.94	17.78	1.58	1.87	0.42	0.20
		AS	0.15	0.22	6.66	5.88	0.15	0.29	0.28	0.12
Chalfant, USA	21/06/1986	MS	0.45	0.40	6.17	8.12	1.94	2.00	0.20	0.74
		AS	0.27	0.24	8.48	11.50	0.53	0.54	0.36	0.40
Mammoth, USA	25/05/1980	MS	0.42	0.44	9.18	9.56	2.25	2.60	0.22	0.14
		AS	0.16	0.18	7.46	7.72	0.24	0.20	0.30	0.34
Whittier, USA	01/10/1987	MS	0.39	0.29	5.70	5.22	0.87	0.81	0.14	0.24
		AS	0.21	0.18	7.82	4.45	0.12	0.16	0.14	0.24

(*Keynote*: MS = Mainshock; AS = Aftershock; SD = Significant Duration; IA = Arias Intensity; P = Predominant Period).

List of figures:

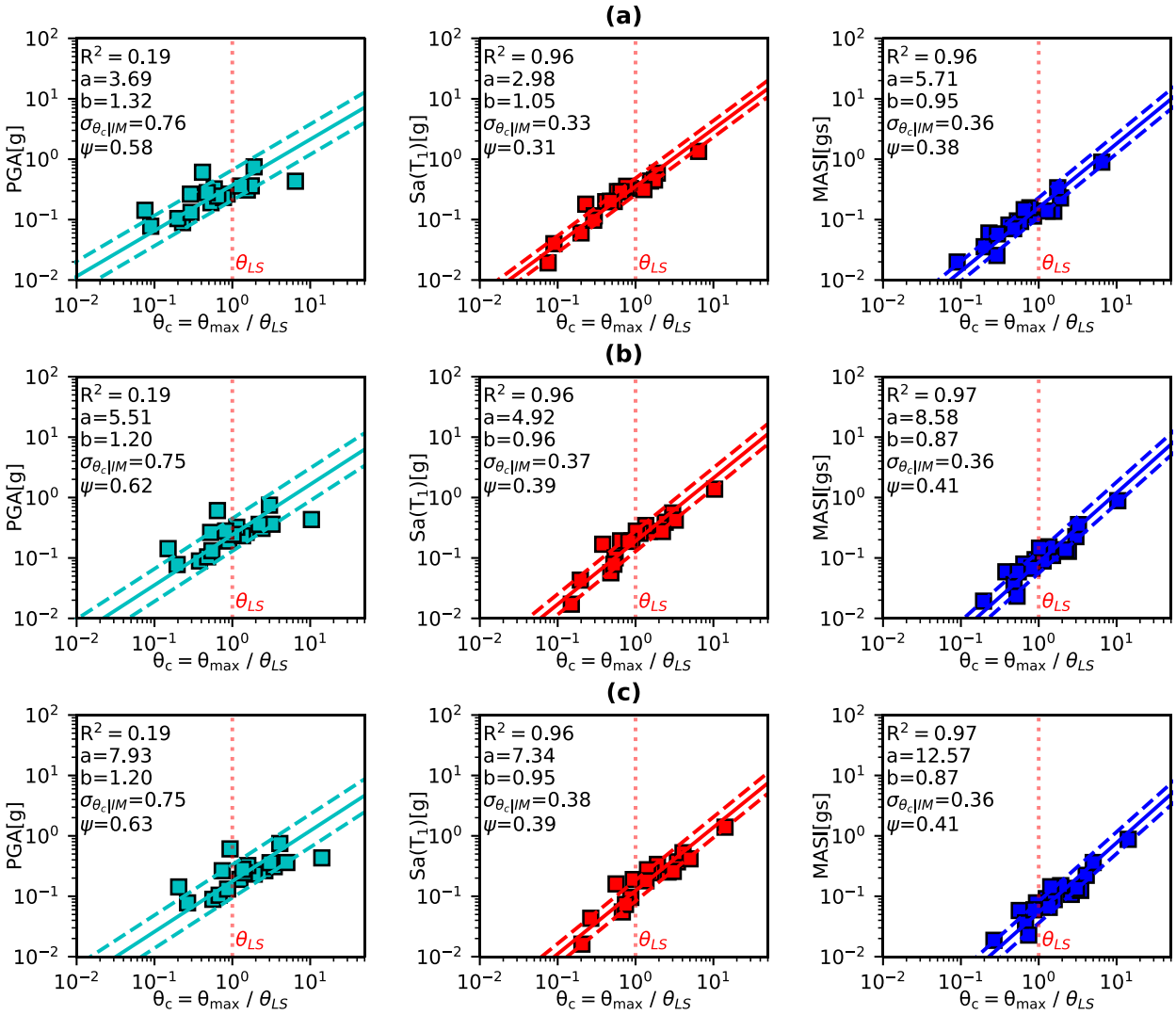

764

765 Figure 17. Numerical relationship between the normalized maximum inter-storey displacement (EDP) and IM (PGA,
766 Sa(T1), MASI) for aftershock motions: (a) CR [%] =0, (b) CR [%] =10, and (c) CR [%] =20%

767

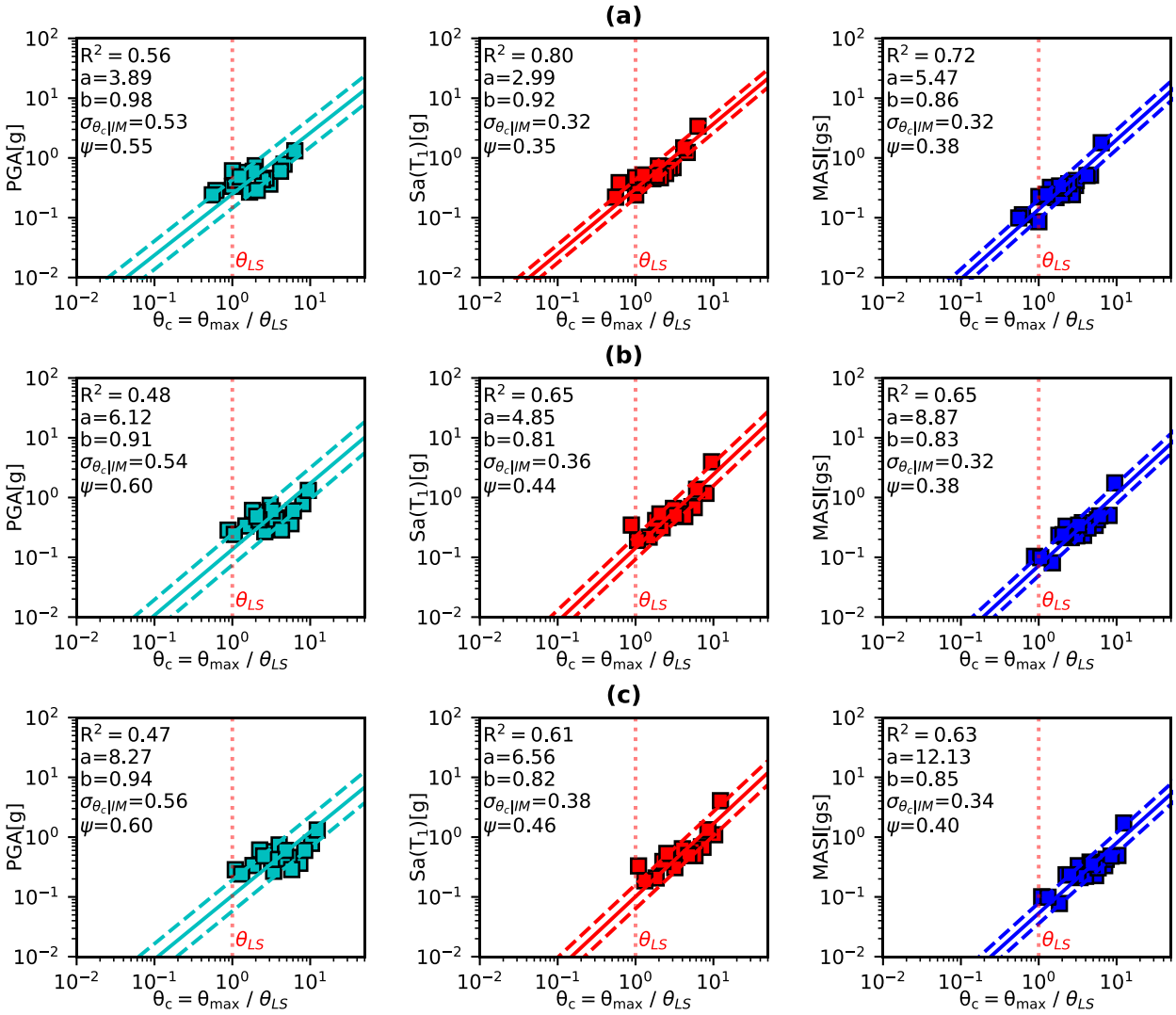

Figure 18.Numerical relationship between the normalized maximum inter-storey displacement (EDP) and IM (PGA, Sa(T1), MASI) for mainshock motions: (a) CR [%] =0, (b) CR [%] =10, and (c) CR [%] =20%

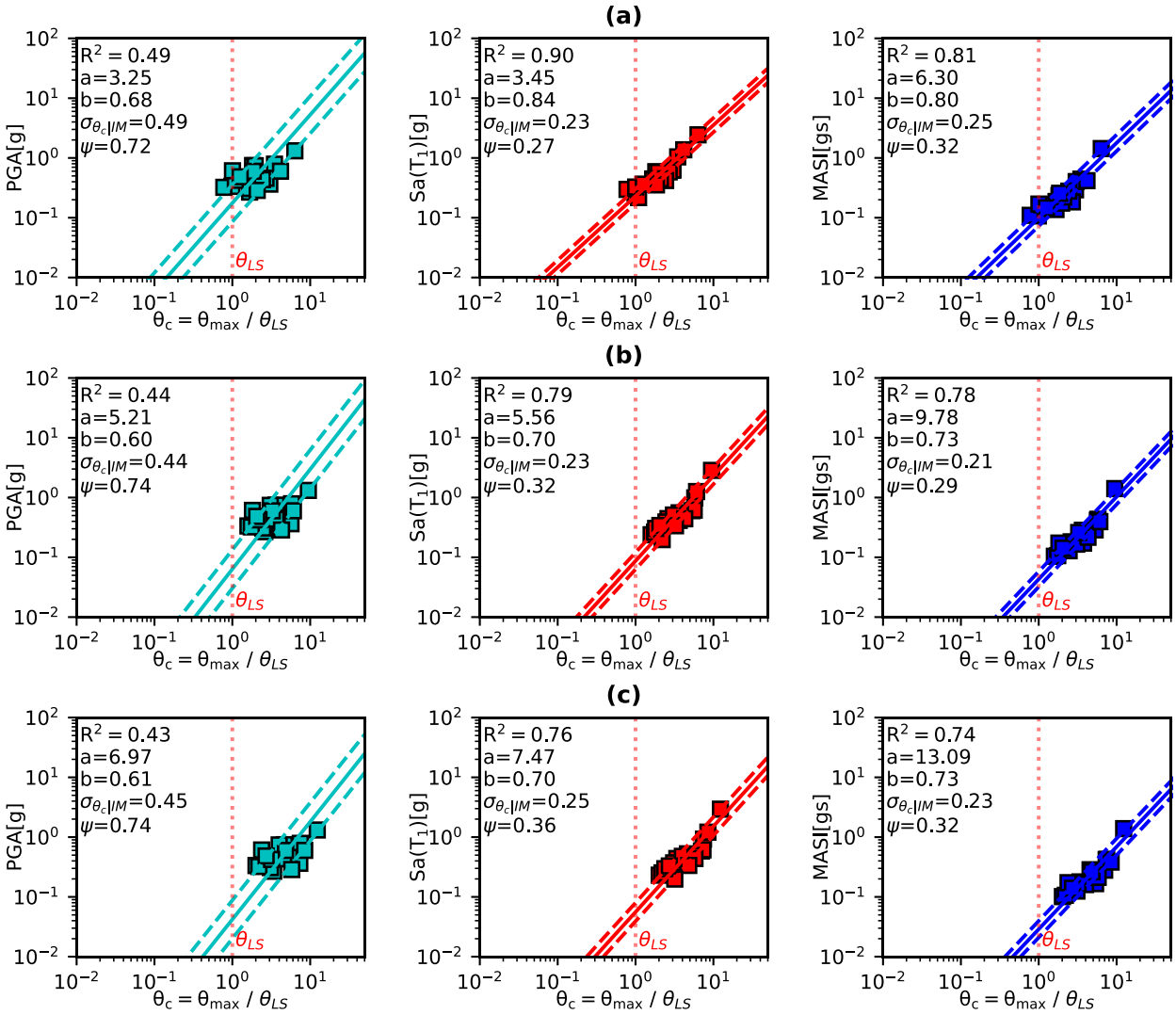

771

772 Figure 19.Numerical relationship between the normalized maximum inter-storey displacement (EDP) and IM (PGA,
773 Sa(T1), MASI) for earthquake sequences: (a) CR [%] =0, (b) CR [%] =10, and (c) CR [%] =20%

774

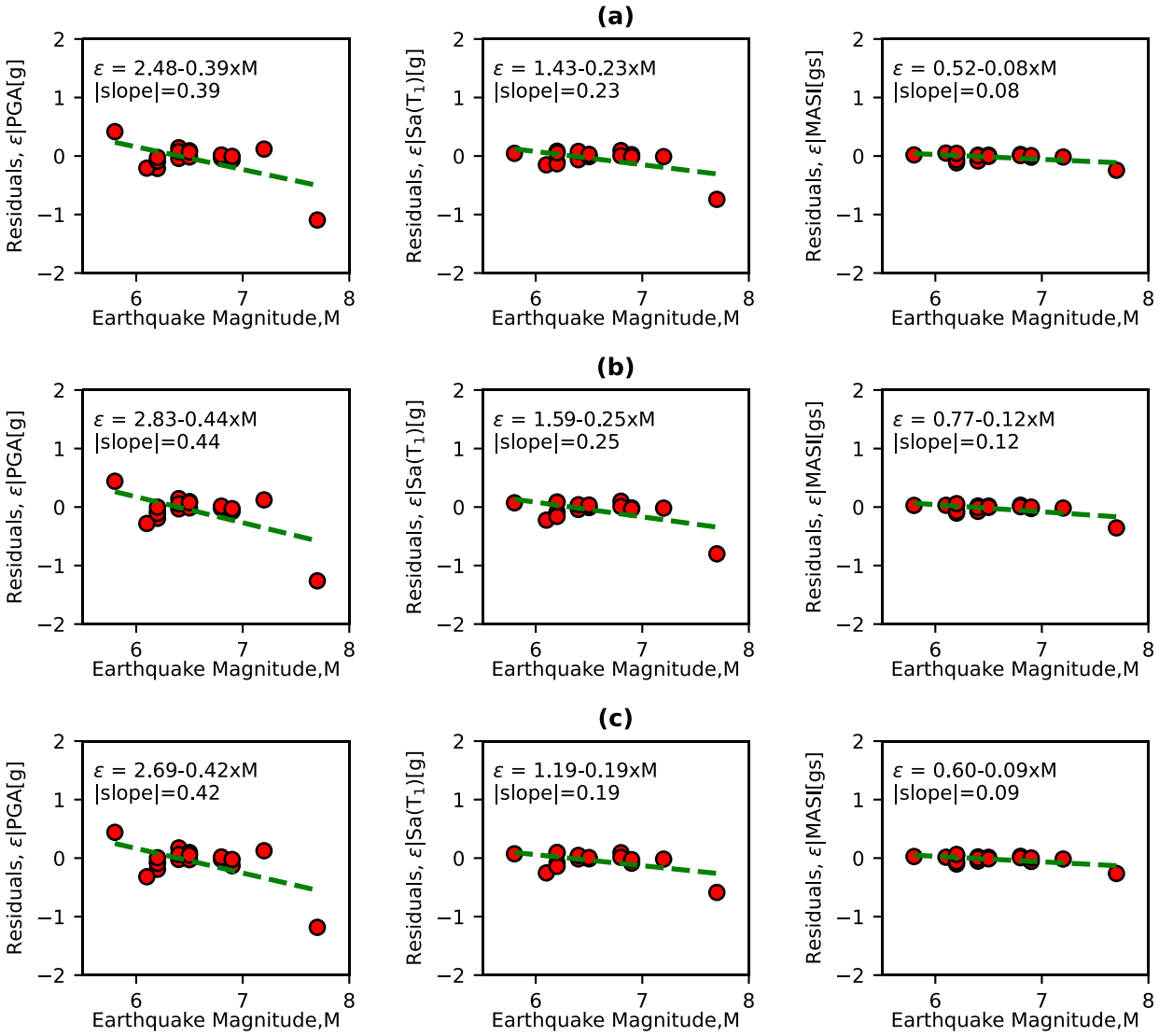

Figure 20. IM residuals versus Earthquake Magnitude: (a) CR [%] =0, (b) CR [%] = 10, and (c) CR [%] = 20

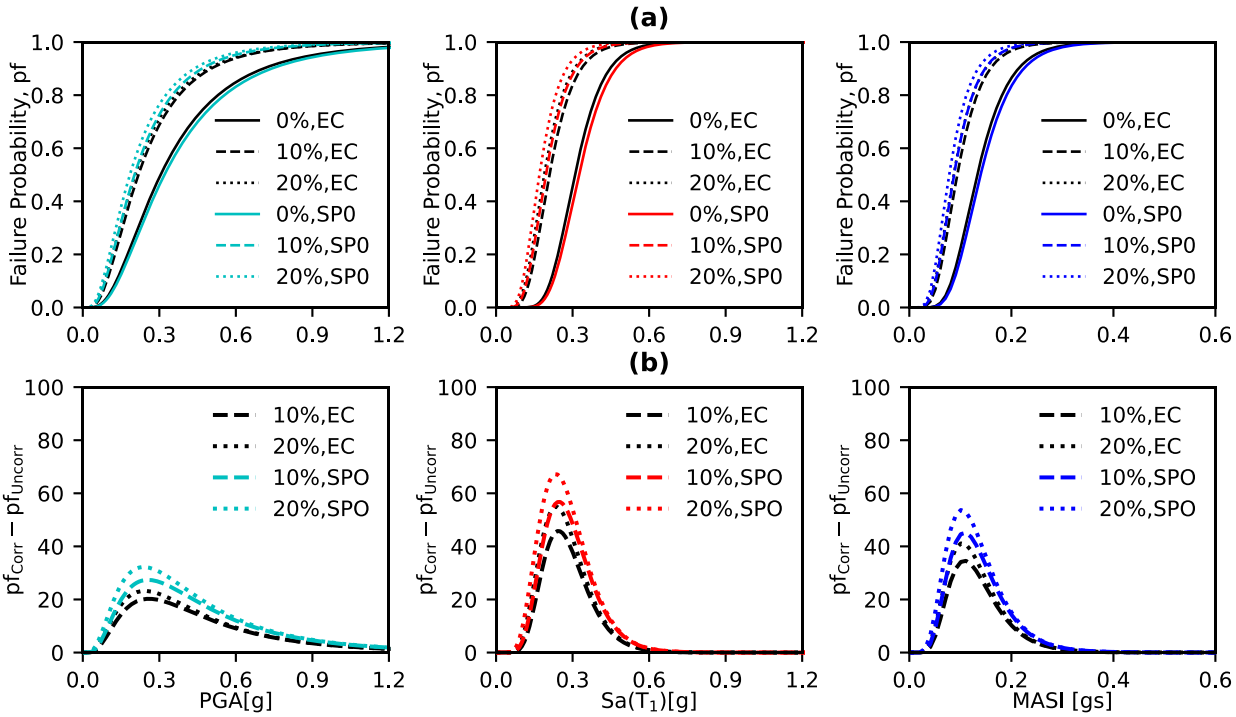

Figure 21. (a) Fragility Curves for aftershock records and (b) Difference of failure probability (CR [%] = 0 as benchmark, *Keynotes*: EC – Eurocode; SPO – Non-Linear Static Pushover Analysis)

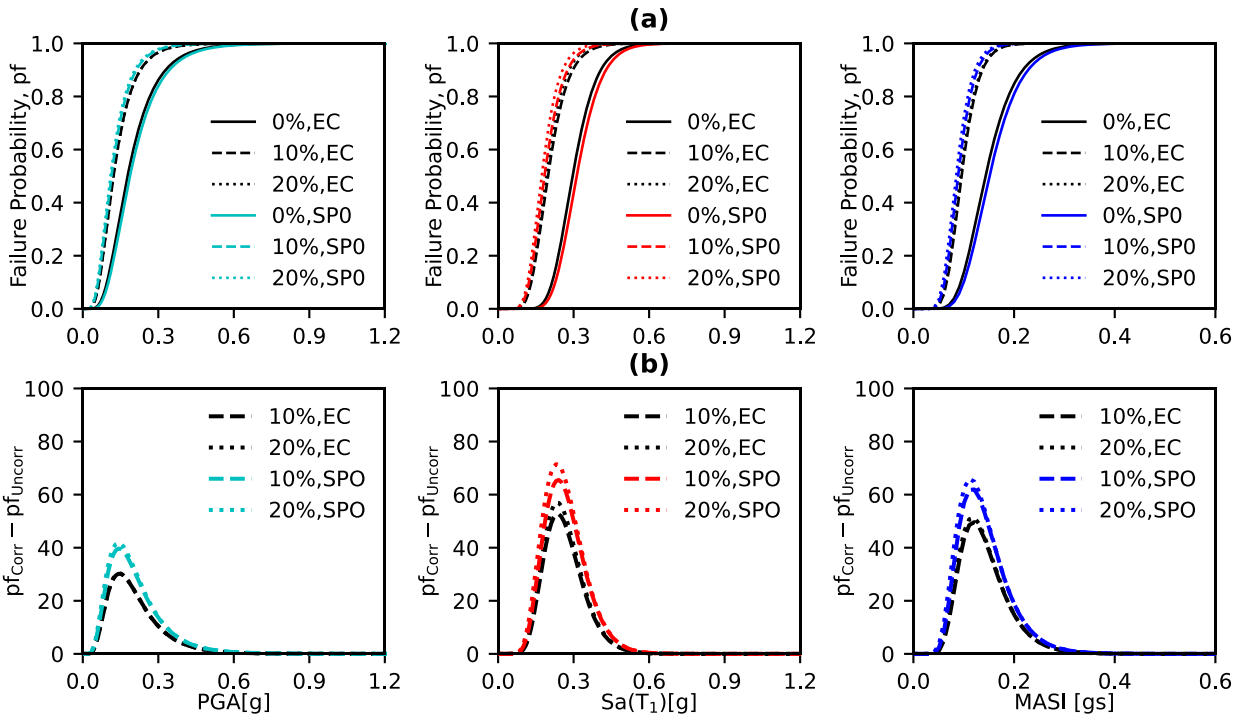

Figure 22. (a) Fragility Curves for mainshock records and (b) Difference of failure probability (CR [%] = 0 as benchmark, *Keynotes*: EC – Eurocode; SPO – Non-Linear Static Pushover Analysis)

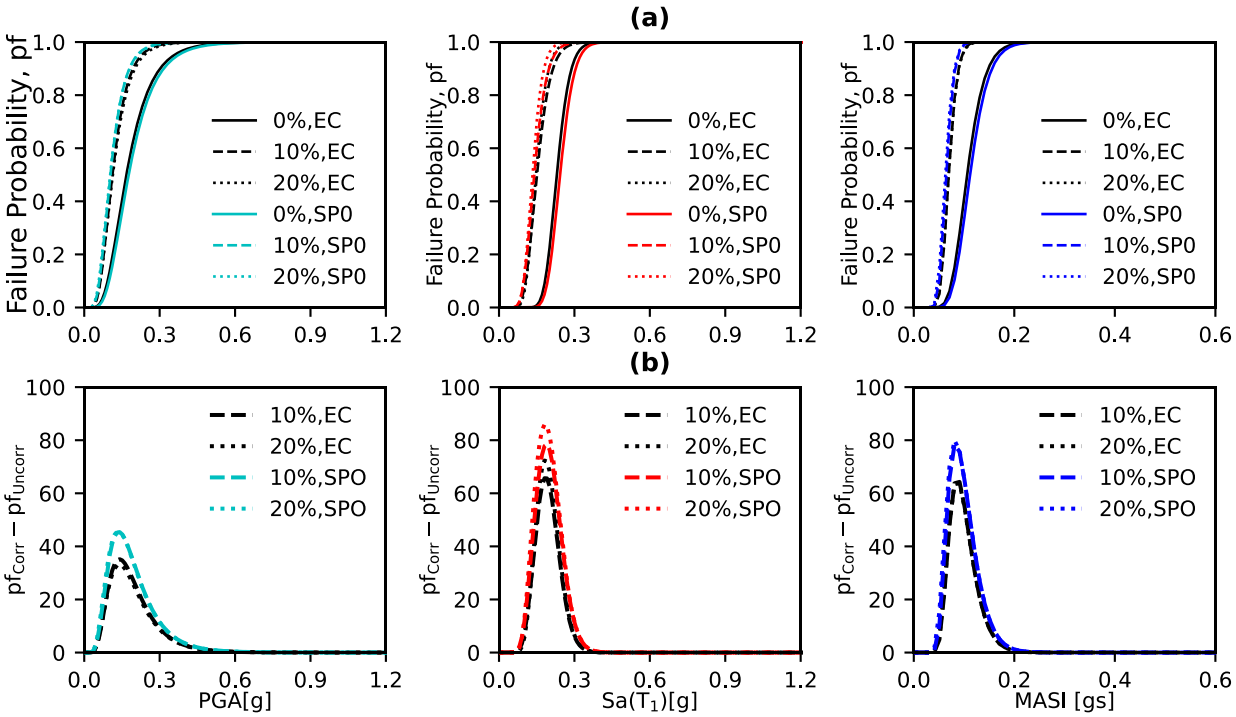

Figure 23. (a) Fragility Curves for sequence records and (b) Difference of failure probability (CR [%] = 0 as benchmark, *Keynotes*: EC – Eurocode; SPO – Non-Linear Static Pushover Analysis)

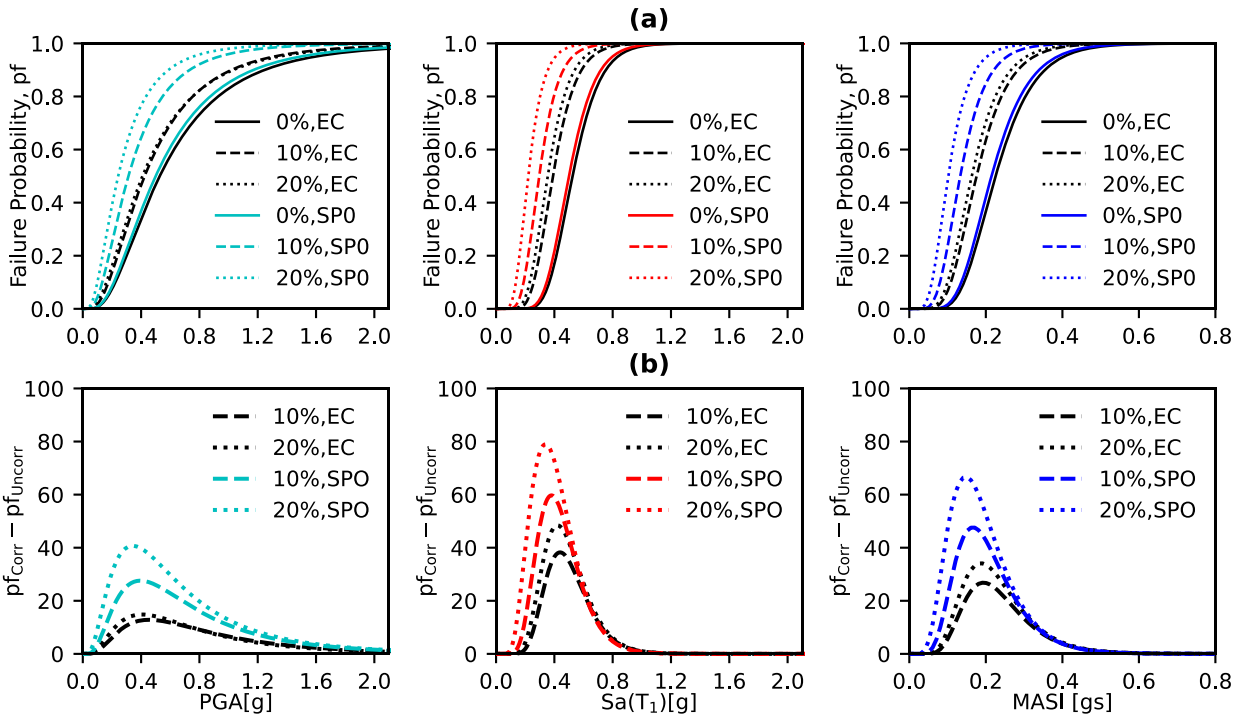

Figure 24. (a) Fragility Curves for aftershock records and (b) Difference of failure probability (CR [%] = 0 as benchmark, *Keynotes*: EC – Eurocode; SPO – Non-Linear Static Pushover Analysis)

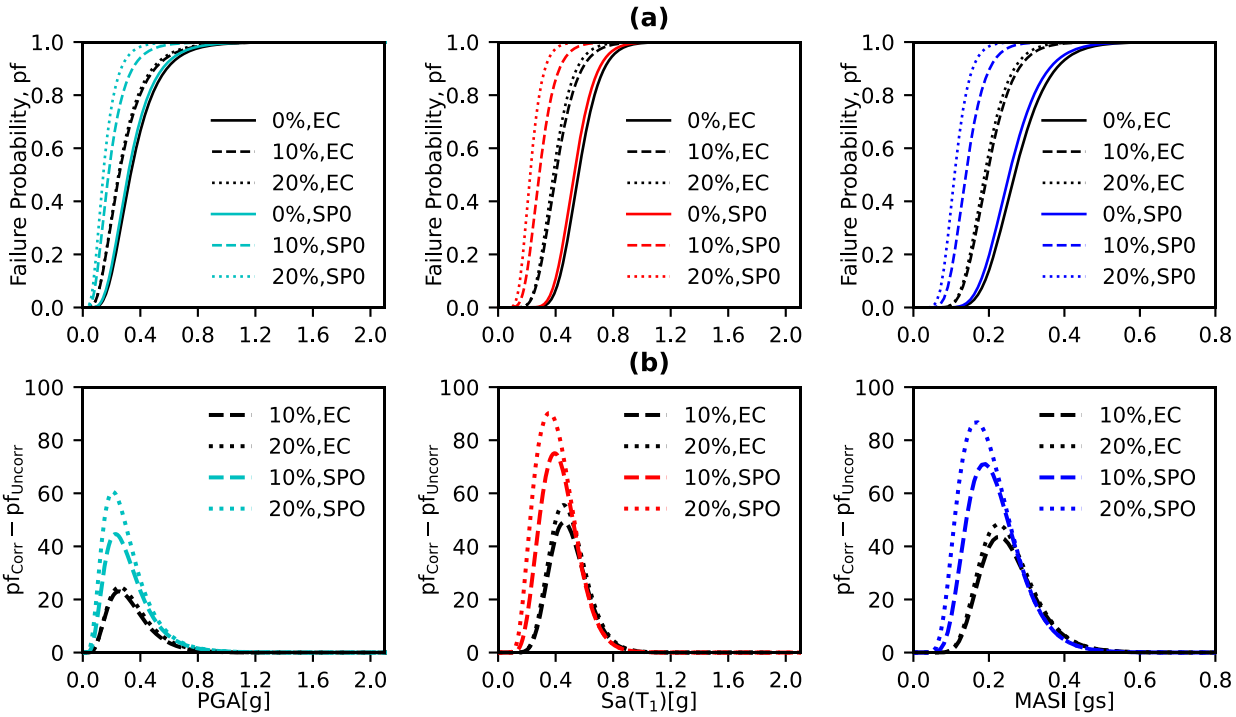

Figure 25. (a) Fragility Curves for mainshock records and (b) Difference of failure probability (CR [%] = 0 as benchmark, *Keynotes*: EC – Eurocode; SPO – Non-Linear Static Pushover Analysis)

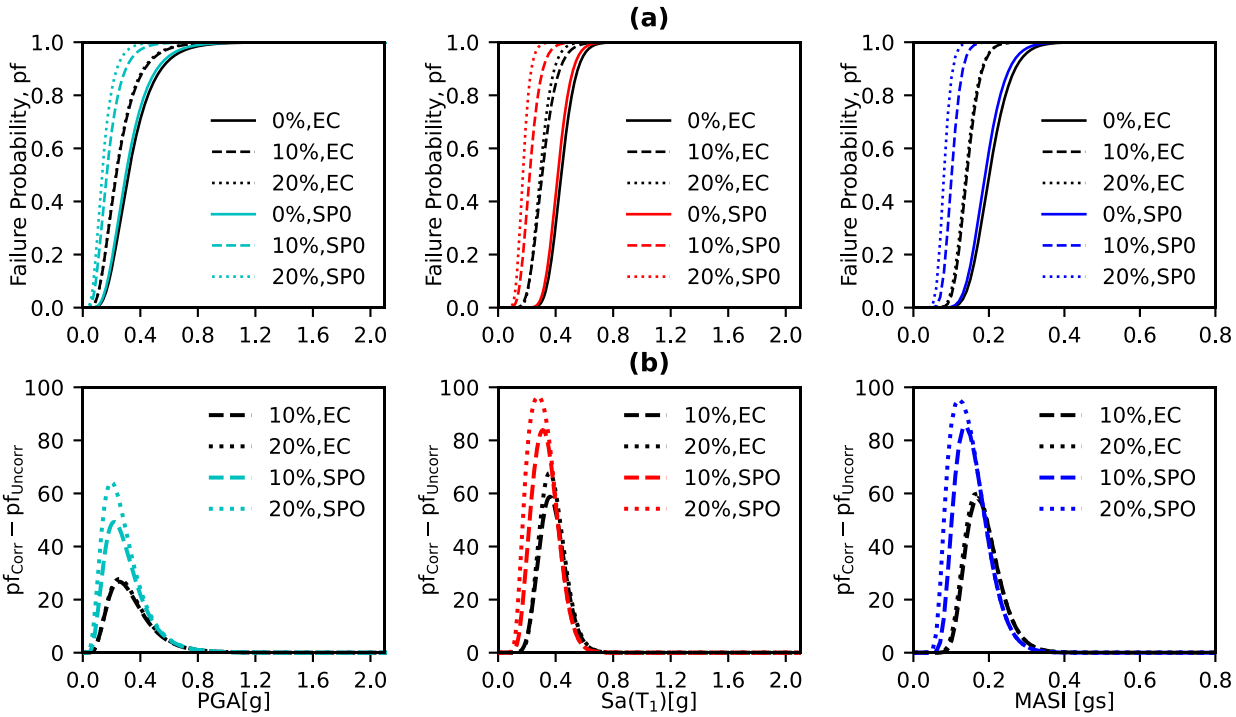

Figure 26. (a) Fragility Curves for sequence records and (b) Difference of failure probability (CR [%] = 0 as benchmark, *Keynotes*: EC – Eurocode; SPO – Non-Linear Static Pushover Analysis)

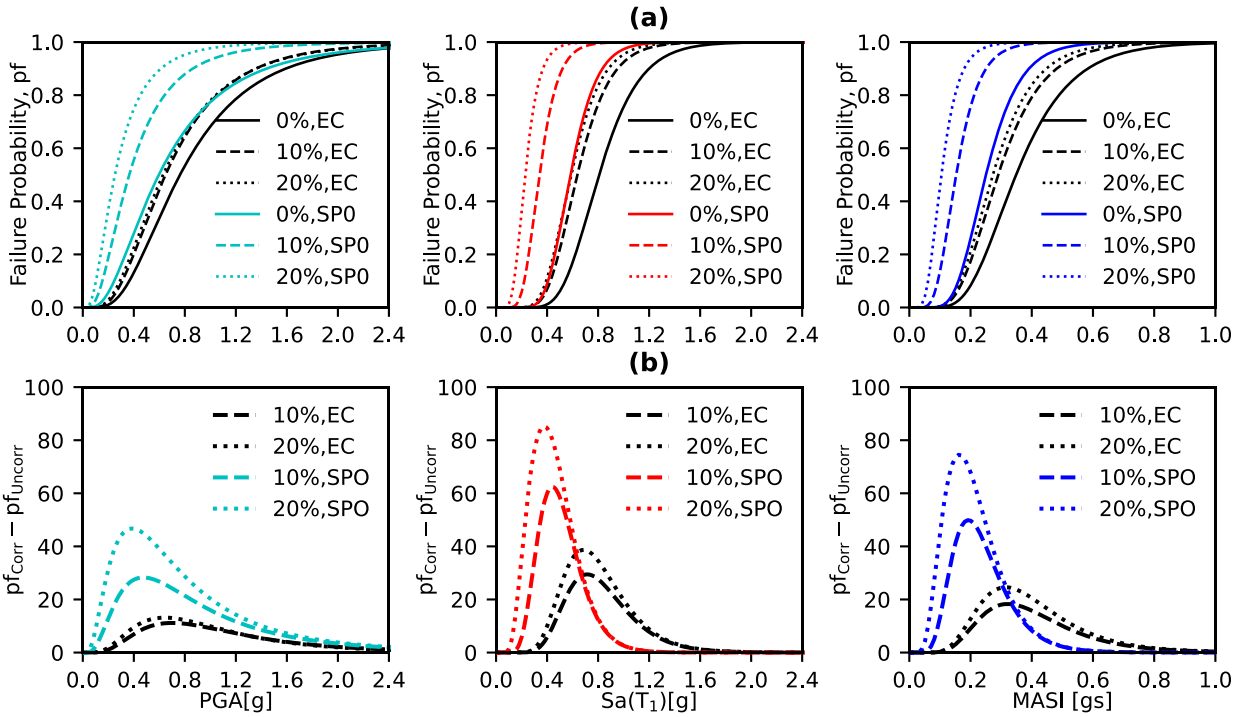

Figure 27. (a) Fragility Curves for aftershock records and (b) Difference of failure probability (CR [%] = 0 as benchmark, *Keynotes*: EC – Eurocode; SPO – Non-Linear Static Pushover Analysis)

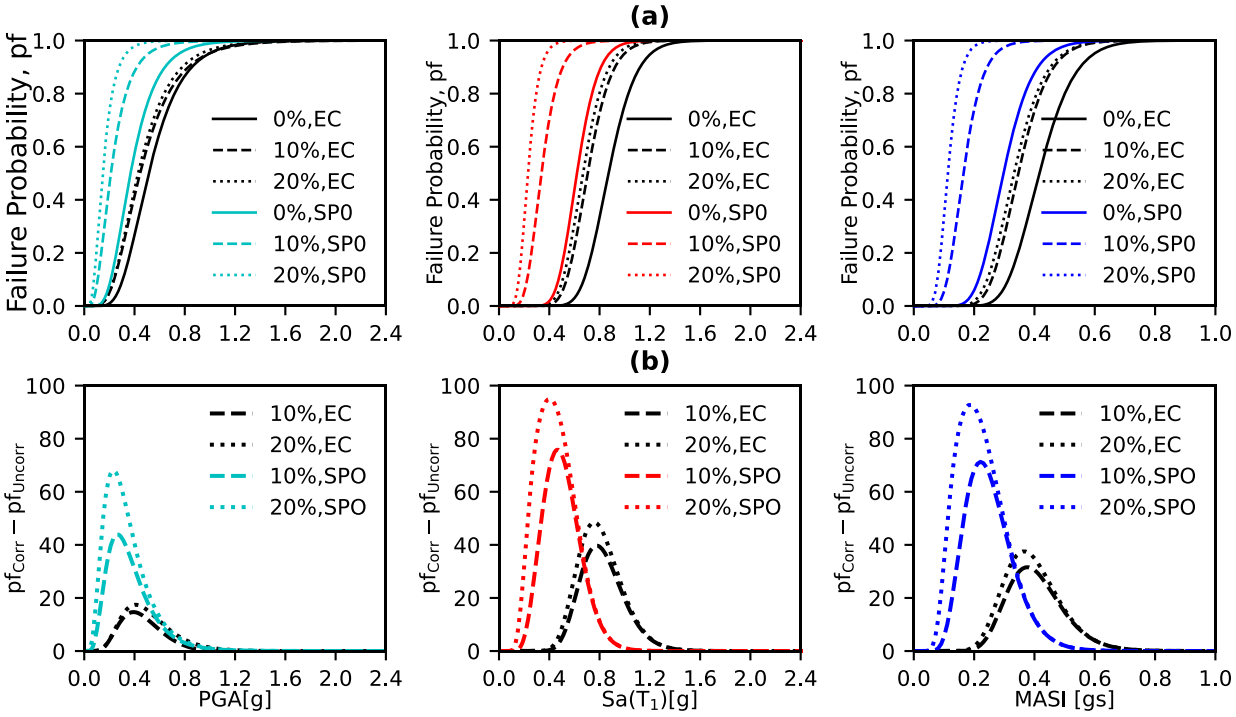

Figure 28. (a) Fragility Curves for mainshock records and (b) Difference of failure probability (CR [%] = 0 as benchmark, *Keynotes*: EC – Eurocode; SPO – Non-Linear Static Pushover Analysis)

807

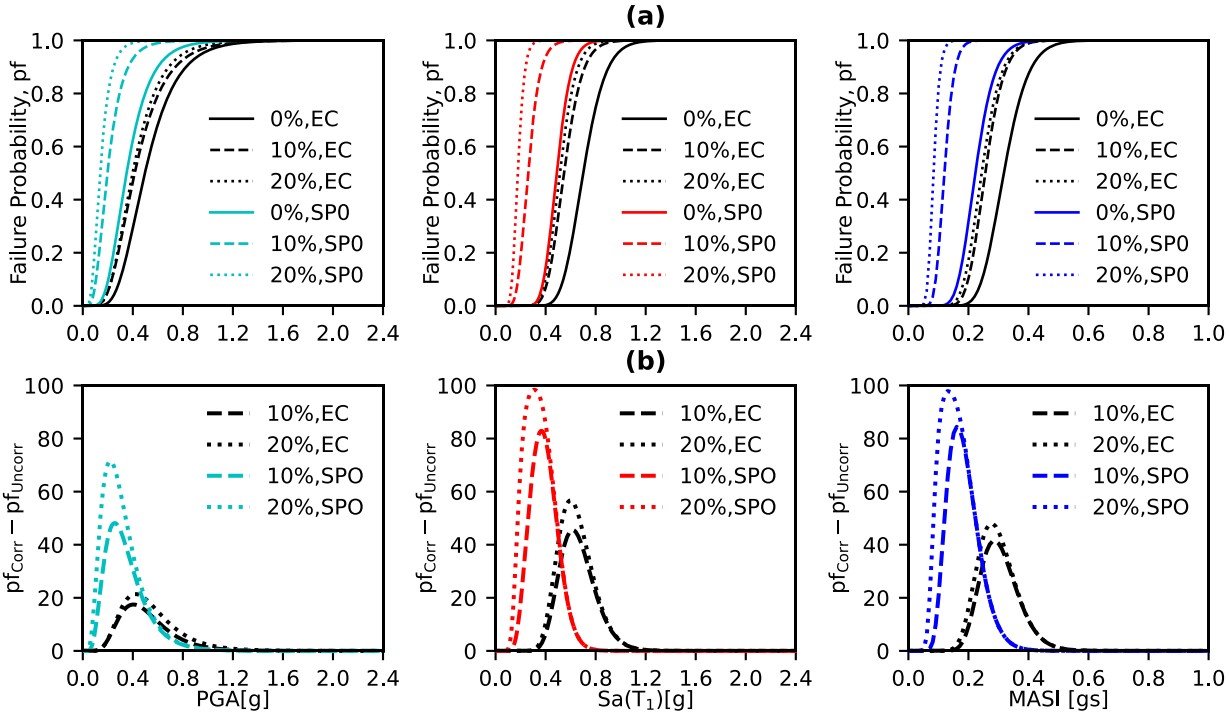

808

809 Figure 29. (a) Fragility Curves for sequence records and (b) Difference of failure probability (CR [%] = 0 as

810 benchmark, *Keynotes*: EC – Eurocode; SPO – Non-Linear Static Pushover Analysis)